Title:

Juvenile social isolation immediately affects the synaptic activity and firing property of fast-spiking parvalbumin-expressing interneuron subtype in mouse medial prefrontal cortex

Authors:

Kazuya Okamura[1], Hiroki Yoshino[1,3,*], Yoichi Ogawa[2], Kazuhiko Yamamuro[1], Sohei Kimoto[1,4], Yasunari Yamaguchi[1,4], Yosuke Nishihata[1], Minobu Ikehara[1], Manabu Makinodan[1], Yasuhiko Saito[2], Toshifumi Kishimoto[1]

Affiliations:

[1]Department of Psychiatry, Nara Medical University, Kashihara, Nara 634-8522, Japan

[2]Department of Neurophysiology, Nara Medical University, Kashihara, Nara 634-8522, Japan

[3]Mie Prefectural Mental Medical Center, Tsu, Mie 514-0818, Japan

[4]Department of Neuropsychiatry, Wakayama Medical University, Kimiidera, Wakayama 641-8509, Japan

***Correspondence:**

Hiroki Yoshino

Department of Psychiatry, Nara Medical University,

840 Shijo-cho Kashihara, Nara 634-8522, Japan

Tel.: +81-744-22-3051;

Fax: +81-744-22-3854;

E-mail: psyosino@naramed-u.ac.jp

Running title: The immediate effect of juvenile social isolation on inhibitory circuits in mPFC

Abstract

A lack of juvenile social experience causes various behavioral impairments and brain dysfunction, especially in the medial prefrontal cortex (mPFC). Our previous studies revealed that juvenile social isolation for two weeks immediately after weaning affects the synaptic inputs and intrinsic excitability of fast-spiking parvalbumin-expressing (FSPV) interneurons as well as a specific type of layer 5 (L5) pyramidal cells, which we termed prominent h-current (PH) cells, in the mPFC. However, since these changes were observed at the adult age of postnatal day 65 (P65), the primary cause of these changes to neurons immediately after juvenile social isolation (postnatal day 35) remains unknown. Here, we investigated the immediate effects of juvenile social isolation on the excitability and synaptic inputs of PH pyramidal cells and FSPV interneurons at P35 using whole-cell patch-clamp recording. We observed that excitatory inputs to FSPV interneurons increased immediately after juvenile social isolation. We also found that juvenile social isolation increases the firing reactivity of a subtype of FSPV interneurons, while only a fractional effect was detected in PH pyramidal cells. These findings suggest that juvenile social isolation primarily disturbs the developmental rebuilding of circuits involving FSPV interneurons and eventually affects the circuits involving PH pyramidal cells in adulthood.

Keywords: electrophysiology, h-current, neurodevelopment, social deprivation, synapse pruning

The medial prefrontal cortex (mPFC) plays a key role in emotion and cognitive functions, including decision-making, language comprehension, attentional selection, and behavioral inhibition (Miller and Cohen 2001; Wood et al. 2003; Dalley et al. 2004). PFC malfunction is related to several psychiatric disorders such as schizophrenia, autism spectrum disorders, and attention-deficit hyperactivity disorder (Arnsten and Rubia 2012; Dienel and Lewis 2019; Xu et al. 2019; Hare and Duman 2020). Early social experiences, such as physical and phonic contacts among fellows, are imperative for brain development, especially the function of the prefrontal cortex (PFC) (Kolb et al. 2012). A lack of juvenile social experiences causes cognitive, emotional, and social dysfunction in adult humans (Egeland et al. 1983; Pollak et al. 2010; Bos et al. 2011). In studies of children reared in foundling hospitals, social deprivation reduces metabolic activity in the temporal and frontal forebrain regions, including the mPFC (Chugani et al. 2001; Eluvathingal et al. 2006). These dysfunctions are irreversible, even if children are moved to a more enriched environment (Chugani et al. 2001). Even in other species, social deprivation causes disorders of sociality and malfunction of the mPFC neural circuit, which persist into adulthood (Harlow et al. 1965; Agrawal et al. 1967; Makinodan et al. 2012; Endo et al. 2018; Yamamuro et al. 2018; Yamamuro et al. 2020a).

We previously reported that juvenile social isolation for two weeks

immediately after weaning at P21 (Early Isolate-Housing; E-IH) reduced the excitatory synaptic inputs and firing properties of a certain type of layer 5 (L5) pyramidal cells in the adult mPFC compared to group-housed (GH) mice (Figure 1A and B) (Yamamuro et al. 2018). We called this subtype of L5 pyramidal cell a prominent h-current (PH) cell because it displayed a prominent h-current (hyperpolarization-activated cation current (Ih)) in response to sustained hyperpolarization. Pyramidal PH cells are characterized by axonal projections to subcortical regions, thicker apical dendrites, and more primary branches than non-PH cells (Dembrow et al. 2010; Gee et al. 2012; Lee et al. 2014).

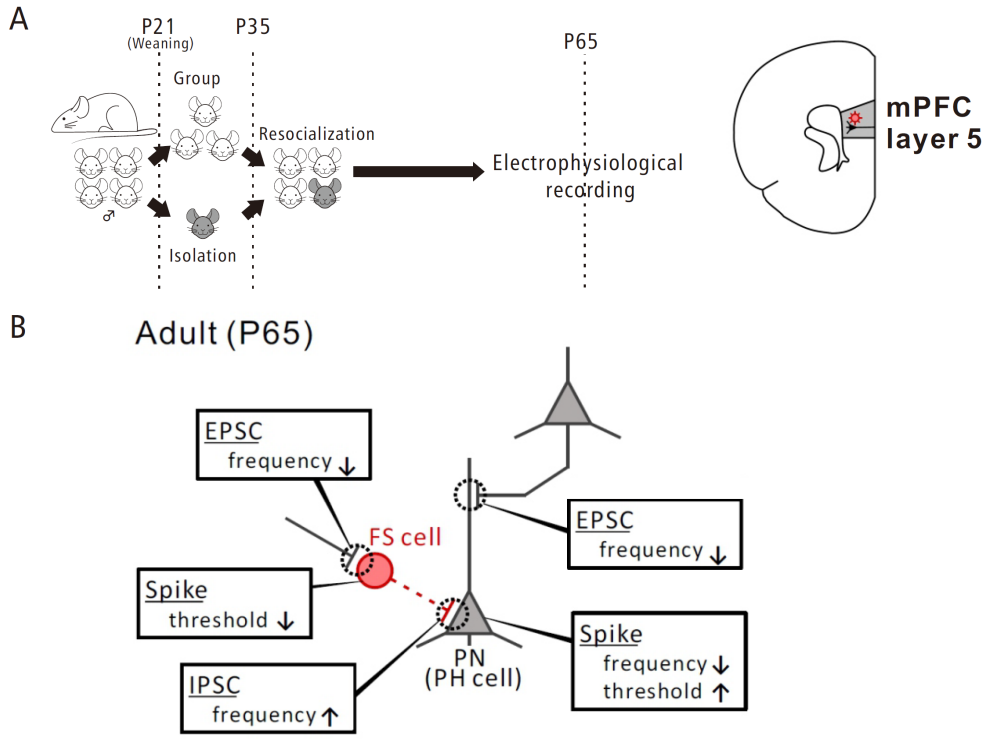

Figure 1.

(A) Left: our previous experimental design of juvenile social isolation and recording. After isolated housing (P21-P35), an isolated mouse was rehoused with the group-reared littermates. Right: a schema showing the whole-cell patch-clamp recording from layer 5 (L5) PH cells (a subtype of pyramidal cell) and L5 FS cells (fast-spiking interneuron) in adult mouse prelimbic cortex at P65. PL: prelimbic cortex. (B) A schema showing the electrophysiological change in the microcircuit of mPFC L5 in the adult mice by juvenile social isolation. Juvenile social isolation decreases excitatory synaptic inputs and increase inhibitory synaptic inputs on PH cell and decrease the excitability of PH cell and decreases excitatory synaptic inputs on FS cell and decrease the excitability of FS cell.

We then explored the effects of E-IH on mPFC inhibitory neuronal circuits in adulthood (Yamamuro *et al.* 2020a). Cortical inhibitory interneurons have been classified into many subclasses based on their distinct morphological, molecular (protein expression), and electrophysiological properties (Markram et al. 2004; Ascoli et al. 2008; Rudy et al. 2011; DeFelipe et al. 2013; Naka and Adesnik 2016; Tremblay et al. 2016). The largest subclass of L5 interneurons in the PFC consists of GABAergic neurons that express parvalbumin (PV) (Gonchar et al. 2007; Xu et al. 2010). PV-expressing GABAergic interneurons are characterized by discriminative

high-frequency firing patterns in response to sustained depolarization, referred to as fast-spiking (FS). Thus, we termed this subclass of GABAergic FSPV interneurons in this study. PFC FSPV cells are believed to regulate the synchrony of pyramidal cell outputs to other brain regions, as well as gamma-oscillatory neuronal activity, which are important for cognitive function (Sohal et al. 2009) because of the reciprocal interaction between PH pyramidal cells and FSPV cells (Kawaguchi et al. 2019). We previously demonstrated that juvenile social isolation increases inhibitory synaptic inputs to PH pyramidal cells and the excitability of FSPV cells, and reduces excitatory synaptic inputs to FSPV cells in adult mice (Yamamuro *et al.* 2020a). Therefore, both excitatory and inhibitory neuronal circuits in the mPFC of adult mice are influenced by juvenile social isolation (Figure 1B). Recent investigations have indicated that juvenile social isolation induces abnormalities in the pyramidal neurons projecting into the posterior paraventricular thalamus (Yamamuro et al. 2020b) and in the parvalbumin-positive interneurons (Bicks et al. 2020) of the mPFC of adult mice. However, no alterations were found immediately after social isolation. Thus, the question remains: what does juvenile social isolation primarily cause? This is crucial to elucidate the concrete process inducing mPFC malfunction due to juvenile social isolation.

Recent reports suggest that FSPV interneurons can be further divided into

subtypes based on their morphological, electrophysiological, and transcriptional features (Gouwens et al. 2020). However, functional differences among these subtypes remain unclear. Juvenile social isolation may selectively affect a specific type of FSPV interneuron.

To investigate these questions, we studied alterations in the network functions of the mPFC immediately after 2-weeks of social isolation (P35) using the whole-cell patch-clamp technique. We focused on the two neuron populations mentioned above, PH pyramidal cells and FSPV interneurons, which are the principal excitatory cells that send subcortical outputs and major intraregional inhibitory cells, respectively. We recorded the membrane potentials and spontaneous postsynaptic currents to assess intrinsic firing ability and synaptic inputs, respectively. We compared these features in PH pyramidal cells and FSPV interneurons prepared from GH and E-IH mice at P35. Initially, we expected that the changes in PH pyramidal cells would begin soon after E-IH. However, contrary to our expectations, the physiological function of PH pyramidal cells was not markedly altered immediately after exposure to social isolation. We found that synaptic inputs to L5 FSPV interneurons were distinctly altered at P35 immediately after social isolation. We also revealed that juvenile social isolation affects firing properties, specifically on a subtype of FSPV interneurons. This study is the first to clarify the primary effects of

juvenile social isolation on the mPFC circuitry during early adolescence.

Material and Methods

Mice and Housing Conditions

C57/BL6 mice were used for the experiments on PH pyramidal cells, and one commercially available transgenic mouse, G42 mouse (CB6-Tg (Gad1-GFP) G42Zjh/J) (Charles River Laboratories, Japan), was used for the experiments on FSPV interneurons. G42 mice express green fluorescent protein (GFP) in subsets of PV-expressing interneurons (Chattopadhyaya et al. 2004). All mice were maintained in a fixed 12-h light-dark cycle. After weaning at P21, four male littermates were randomly divided into one isolated mouse and three group-reared mice. The isolated mouse was individually housed from P21 to P35 (Yamamuro *et al.* 2018; Yamamuro *et al.* 2020a). In the re-socialization period, the isolated mouse was housed with its three littermates until P65 (Figure 1A). In experiments using C57 mice, recordings were made at P21, P35, and P65; in experiments using G42 mice, recordings were made at P21 and P35. Furthermore, among G42 mice, only GFP-positive mice were used to compare E-IH and GH. All experiments were approved by the Animal Care and Use Committee of Nara Medical University and were conducted according to the guidelines.

Electrophysiology

Brain slices, including the mPFC, were prepared from 20- to 22-day-old, 33- to 37-day-old, and 63- to 70-day-old mice. Mice were deeply anesthetized with isoflurane and decapitated. The brain was quickly removed and immersed in ice-cold sucrose-based solution bubbled with a mixed gas of 95% O_2/ 5% CO_2, containing (in mM): 230 sucrose, 2.5 KCl, 25 $NaHCO_3$, 1.25 NaH_2PO_4, 0.5 $CaCl_2$, 10 $MgSO_4$, and 10 D-glucose. The frontal cortex was sectioned into 300-330μm-thick slices in the coronal plane using a vibrating tissue slicer (Vibratome 1000 Plus 102, Pelco International). Slices were incubated for at least 60 min in a chamber filled with a standard artificial cerebrospinal fluid (ACSF) continuously bubbled with a mixed gas containing (in mM): 125 NaCl, 2.5 KCl, 25 $NaHCO_3$, 1.25 NaH_2PO_4, 2 mM $CaCl_2$, 1 mM $MgCl_2$, and 25 mM D-glucose at 32 °C, and then maintained in the ACSF at 25 °C. Following incubation, the slice was transferred to a recording chamber, where the submerged slice was superfused at a flow rate of 2mL per min with ACSF saturated with the mixed gas at 32 °C.

Electrophysiological data were recorded from PH pyramidal cells and FSPV interneurons located in L5 of the mPFC (the prelimbic and infralimbic cortices). Slices were visualized on video images using an upright microscope (BW50WI, Olympus)

with infrared differential interference contrast (IR-DIC) optics for recording PH pyramidal cells. Each pyramidal cell was identified by its morphological features, that is, large pyramidal or oval cell bodies and thick apical dendrites. To identify FSPV interneurons, slices were imaged with an upright microscope (DM6000 FS, Leica) equipped with both epifluorescence illuminator and IR-DIC optics. In slices prepared from G42 mice, each L5 FSPV interneuron was first identified by its green (GFP) fluorescence and its cell body was determined using the IR-DIC view.

Cells were voltage- and current-clamped in a conventional whole-cell configuration using a Multiclamp 700A amplifier (Axon Instruments). Patch pipettes were pulled from borosilicate glass and filled with a low-chloride intracellular solution containing (in mM): 141 K-gluconate, 4 mM KCl, 2 mM $MgCl_2$, 2 Mg-ATP, 0.3 Na-GTP, 0.2 EGTA, 10 mM HEPES, pH 7.25, adjusted with KOH to record excitatory postsynaptic currents (EPSCs). To record inhibitory postsynaptic currents (IPSCs), we used a high-chloride intracellular solution containing (in mM): 95 K-gluconate, 50 mM KCl, 2 mM $MgCl_2$, 2 Mg-ATP, 0.3 Na-GTP, 0.2 EGTA, 10 mM HEPES, pH 7.25 adjusted with KOH. All membrane potentials were corrected for liquid junction potential (13 mV and 7 mV for the low- and high-chloride pipet solutions, respectively) measured according to previously established methodology (Neher 1992). The equilibrium potentials for chloride ions, which are equivalent to reversal potentials for

GABAA-receptor-mediated current, were calculated to be -74 and -24 mV in our experimental arrangements with low- and high-chloride pipet solutions, respectively. Data acquisition and stimulation were controlled using Signal 4 software with Power 1401 interface equipment (Cambridge Electronic Design).

Voltage-Clamp Recording

In the voltage-clamp recording, the pipette capacitance was compensated, and series resistance was continuously monitored and not compensated. Only recordings with a stable series resistance < 20 MΩ were used for analyses. Current signals were low-pass filtered at 600 Hz and digitized at a sampling frequency of 10kHz. To record postsynaptic currents, the recording cells were held at –70mV.

We recorded spontaneous EPSCs (sEPSCs) in the ACSF without $GABA_A$ receptor antagonists to maintain both excitatory and inhibitory neuronal activity in the slice. Under our experimental conditions using the low-chloride pipet solution, $GABA_A$ receptor-mediated postsynaptic currents were outward and too small to be detected in most events, whereas EPSCs were detected as definite inward currents. Tetrodotoxin (TTX)-resistant miniature EPSCs (mEPSC) were recorded in the presence of 10μM gabazine and 1μM TTX.

Under the experimental conditions using the high-chloride pipette solution for

recording IPSCs, glutamate receptor-mediated inward currents were blocked by administrating 10μM CNQX, an AMPA/ kainate-receptor antagonist, and 10μM D-AP5, an NMDA receptor antagonist to the ACSF. $GABA_A$ receptor-mediated currents were detected as prominent inward currents. We also recorded miniature IPSCs (mIPSCs) in the presence of 10μM CNQX, 10μM D-AP5, and 1μM TTX.

Current-Clamp Recording

For the current-clamp recordings, series resistance was monitored and canceled using a bridge circuit, and pipette capacitance was compensated. Voltage signals were low-pass filtered at 10kHz and digitized at 20kHz. The baseline membrane potential was maintained near -70mV with current injection.

To examine action potentials and subthreshold membrane properties, we recorded membrane potential responses to hyperpolarizing and depolarizing current pulses (500ms in duration). Depolarizing current pulses with intensities of 10 – 200 pA were injected in increments of 10 pA.

Hyperpolarizing current pulses with intensities of -10 to -200 pA were injected at a -10 pA step. We assessed the h-current magnitude as the voltage sag at hyperpolarization induced by a -50pA current injection and calculated the sag ratio as previously described (Yamamuro et al. 2018). Then, we categorized pyramidal cells

with > 5% sag ratio as prominent h-current cells (PH cells), and the other cells as non-PH cells (Yamamuro *et al.* 2018; Yamamuro *et al.* 2020a). We also defined FSPV cells with > 5% sag ratio as type A cells and the other cells as type B cells, according to the classification by Gouwens et al. (Gouwens et al. 2020).

Cell Labeling

The pipette solution usually contained 1.5% biocytin for morphological examination. After pipette withdrawal, slices were fixed in 4% paraformaldehyde in phosphate-buffered saline (PBS) overnight. After overnight permeabilization with 0.25% Triton X-100 in PBS, slices were incubated with streptavidin-conjugated Alexa 555 (diluted 1:250 in PBS containing 0.1% Triton X-100) for 6 h. The slices were then rinsed and cleared using SeeDB2 protocol (Ke et al. 2016). Biocytin-labeled cells were imaged using a confocal laser scanning microscope (FV1000, Olympus, Tokyo, Japan).

Immunochemistry

Mice were deeply anesthetized and perfused transcardially with 4% paraformaldehyde. Immunohistochemical staining was performed using primary antibodies for 24 h at 4 °C after blocking for 30 min at room temperature with 5% goat

serum (Chemicon). Cryostat sections were incubated with Alexa Fluor ® secondary antibodies (Thermo Scientific) for 1 h at room temperature. The primary antibodies used to visualize G42-and PV-expressing cells were anti-GFP (A5455, Thermo Scientific) and anti-PV (MAB1572, Merck). Images were captured using a BZX-710 fluorescence microscope (Keyence, Tokyo, Japan).

Data Analyses

We analyzed the membrane potential data obtained from the current-clamp recordings using Signal 4 software and evaluated the intrinsic membrane and action potential properties of each cell. The input resistance of the neurons was estimated using the linear regression coefficient for changes in peak voltage due to injected hyperpolarizing currents (-50 pA to -10 pA, 500ms). The rheobase (current threshold) was defined as the minimum current value at which the current injection elicited at least an action potential. For the action potential elicited by the rheobase current injection, the action potential threshold was measured using the derivatives of the voltage curve. The action potential threshold was defined as the voltage at which the slope of the action potential trace was 10 mV/ms. Spike amplitude was defined as the voltage from the threshold to the peak of the action potential at the rheobase. The rheobase and voltage threshold are indicative of excitability, that is, the ability to

detect a small input. We also examined the firing reactivity of neurons as another property involved in firing capacity. For evaluating the firing reactivity of neurons, that is, the ratio of firing output to current input, we measured the frequencies of action potentials in response to depolarizing current injections (+10 pA to +140 pA from the rheobase) and examined the curvilinear relations between the frequencies of spikes (F-I relation). We did not apply repeated-measures analysis of variance (ANOVA) as a statistical test for the F-I relations because the circularity of the variance-covariance matrix, which is an assumption of repeated-measures ANOVA, was not valid (Mauchly test). Instead, we applied the Student's t-test or Mann–Whitney U test to spike frequency at 100 pA larger than the rheobase for analyzing differences in F-I relation since the curved forms of F-I relation were almost analogous to each other except for the slope. In this paper, we have referred to this measurement as spike frequency for simplicity. We used Mini Analysis software (Synaptosoft) to detect and analyze sEPSCs, mEPSCs, sIPSCs, and mIPSCs on the membrane current data obtained from the voltage-clamp recordings. For each cell, all PSCs for 2.5 min were detected and the mean amplitude and frequency were calculated.

Data are presented as means ± standard error of the mean (SEM), and standard bar charts or line plots were used. Statistical analyses were performed using Prism version 8 (GraphPad). Significant differences were determined using the

Student's *t*-test (normal distribution) or Mann–Whitney *U* test (non-normal distribution) between two groups. One-way analysis of variance (ANOVA), followed by Tukey's honest significant difference (HSD) test (normal distribution) or Kruskal-Wallis test followed by Dunn's test (non-normal distribution), was used for comparison between three groups. All statistical tests were two-tailed. Differences between group means or medians were considered significant at $p < 0.05$.

Results

The functional change of PH pyramidal cells with normal development.

Generally, the physiological functions of cortical pyramidal cells mature and change during development (McCormick and Prince 1987; Zhang 2004). In our previous report, malfunction of mPFC PH pyramidal cells and behavioral abnormalities affected by juvenile social isolation were found in adulthood (P65). One of the aims of this study was to investigate the effects of juvenile social isolation on PH pyramidal cells during the early developmental period (P35). However, how PH pyramidal cells functionally develop from weaning (P21) to adulthood (P65) remains unknown. First, to examine how the physiological function of PH pyramidal cells changes with normal development, we evaluated their excitability and synaptic inputs at three different postnatal days (P21, P35, and P65). Action potential properties were

analyzed at each developmental stage (Figure 2A and B). There were no significant differences in spike amplitudes (Figure 2C). The frequency of the spikes increased with development (Figure 2D). However, this trend was not significant. The spike threshold decreased significantly with development (Figure 2E). These results are consistent with those of a previous study that investigated PFC L5 pyramidal neurons in rats (Zhang 2004). Regarding developmental changes in synaptic function (Figure 2F), there were no significant differences in sEPSC amplitude, sEPSC frequency (Figure 2G), mEPSC amplitude, or mEPSC frequency among developmental stages (Figure 2H). These results indicate that the excitability of L5 PH pyramidal cells increases developmentally by lowering the spike threshold, whereas the excitatory synaptic input onto L5 PH cells does not quantitatively change during this developmental period after weaning.

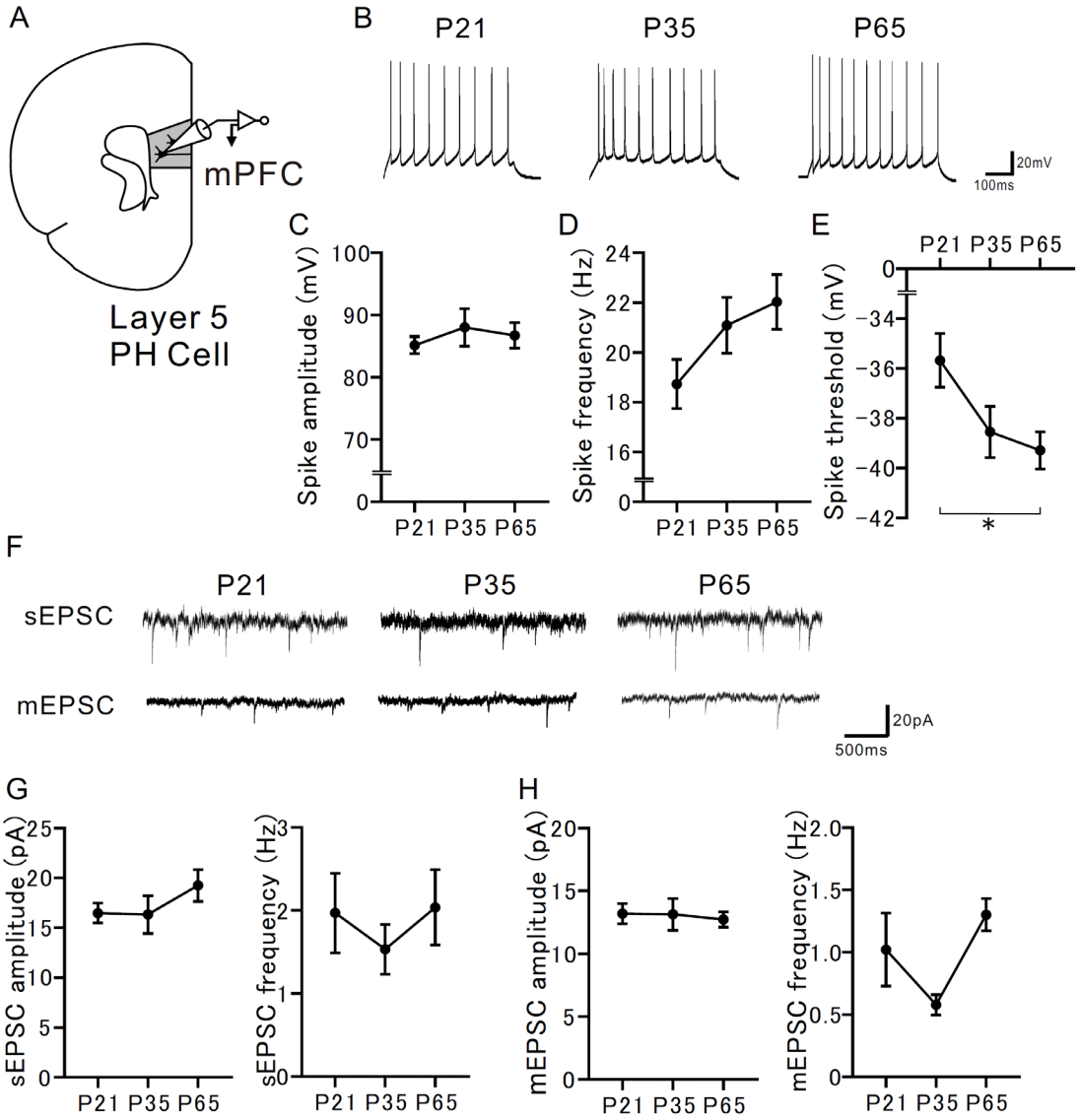

Figure 2.

(A) A schema showing the whole-cell patch-clamp recording from L5 PH cells in the mouse prelimbic cortex.

(B) Representative spikes elicited by a current injection of 100-pA larger than the rheobase recorded from PH cells at P21, P35, and P65 in normal development.

(C-E) The normal developmental changes in firing properties of PH cells.

(C) Spike amplitude did not change during development (one-way ANOVA, $F_{2, 41}$ = 0.2635, P = 0.7697, n = 10 (P21), 11 (P35), 23 (P65)).

(D) Spike frequency did not change during development (one-way ANOVA, $F_{2, 41}$ = 1.854, P = 0.1696, n = 10 (P21), 11 (P35), 23 (P65)).

(E) Spike threshold significantly decreased during development (Kruskal-Wallis, χ^2 = 7.222, *P = 0.0270; Dunn's test: P21 versus P35, P = 0.1444; P21 versus P65, *P = 0.0245; P35 versus P65, P > 0.9999; n = 10 (P21), 11 (P35), 23 (P65)).

(F) Representative traces showing sEPSCs (top) and mEPSCs (bottom) recorded from PH cells at P21 (left), P35 (middle) and P65 (right).

(G) There were no differences in the sEPSC amplitude (left) (one-way ANOVA, $F_{2, 24}$ = 1.329, P = 0.2835) or sEPSC frequency (right) during development (one-way ANOVA, $F_{2, 24}$ = 0.2771, P = 0.7604, n = 10 (P21), 6 (P35), 11 (P65)).

(H) There were no differences in the mEPSC amplitude (left) (one-way ANOVA, $F_{2, 36}$ = 0.1146, P = 0.8921) or mEPSC frequency (right) during development (one-way ANOVA, $F_{2, 36}$ = 2.872, P = 0.0696, n = 10 (P21), 6 (P35), 11 (P65)).

*P < 0.05. Data are represented as means and error bars indicate SEM.

Juvenile social isolation partially affected the firing capacity of PH pyramidal cell at the early stage (P35).

We previously reported that juvenile social isolation increases the spike threshold and reduces the firing reactivity of mPFC L5 PH pyramidal cells in adult mice. Our previous studies also revealed a decrease in EPSC frequency and an increase in IPSC frequency in mPFC PH pyramidal cells in adult mice (Figure 1B) (Yamamuro *et al.* 2018; Yamamuro *et al.* 2020a). These changes may appear at an earlier stage, immediately after juvenile social isolation. To investigate this possibility, we examined the firing properties and excitatory and inhibitory synaptic inputs into PH pyramidal cells at P35, that is, immediately after social isolation in E-IH mice (Figure 3A). After confirming no difference in the distribution of the magnitude of h-current (sag ratio) between GH and E-IH mice (Figure 3B), the firing properties of PH pyramidal cells were evaluated (Figure 3C-J). There were no significant differences between E-IH and GH mice in spike threshold (Figure 3G), spike amplitude (Figure 3H), spike half-width (Figure 3I), and input resistance (Figure 3J). However, in E-IH mice, the spike frequency in response to depolarizing current injection decreased significantly (Figure 3D and E), and the rheobase increased significantly (Figure 3F). These findings indicate that juvenile social isolation at least partially reduces the firing capacity of PH pyramidal cells already at P35. Regarding synaptic inputs, there was no significant difference in the frequency and amplitude of sEPSCs and TTX-resistant mEPSCs between the E-IH and GH mice (Figure 3K-M). Furthermore, no significant

differences in amplitude and frequency were detected between sIPSCs and mIPSCs (Figure 3N-P), immediately after juvenile social isolation. These results indicate that the inhibitory effects of juvenile social isolation on the firing capacity of PH pyramidal cells begin to partially manifest at an early stage immediately after isolated housing. Meanwhile, we did not find any alterations in excitatory and inhibitory inputs on PH cells due to juvenile social isolation in PH cells at P35.

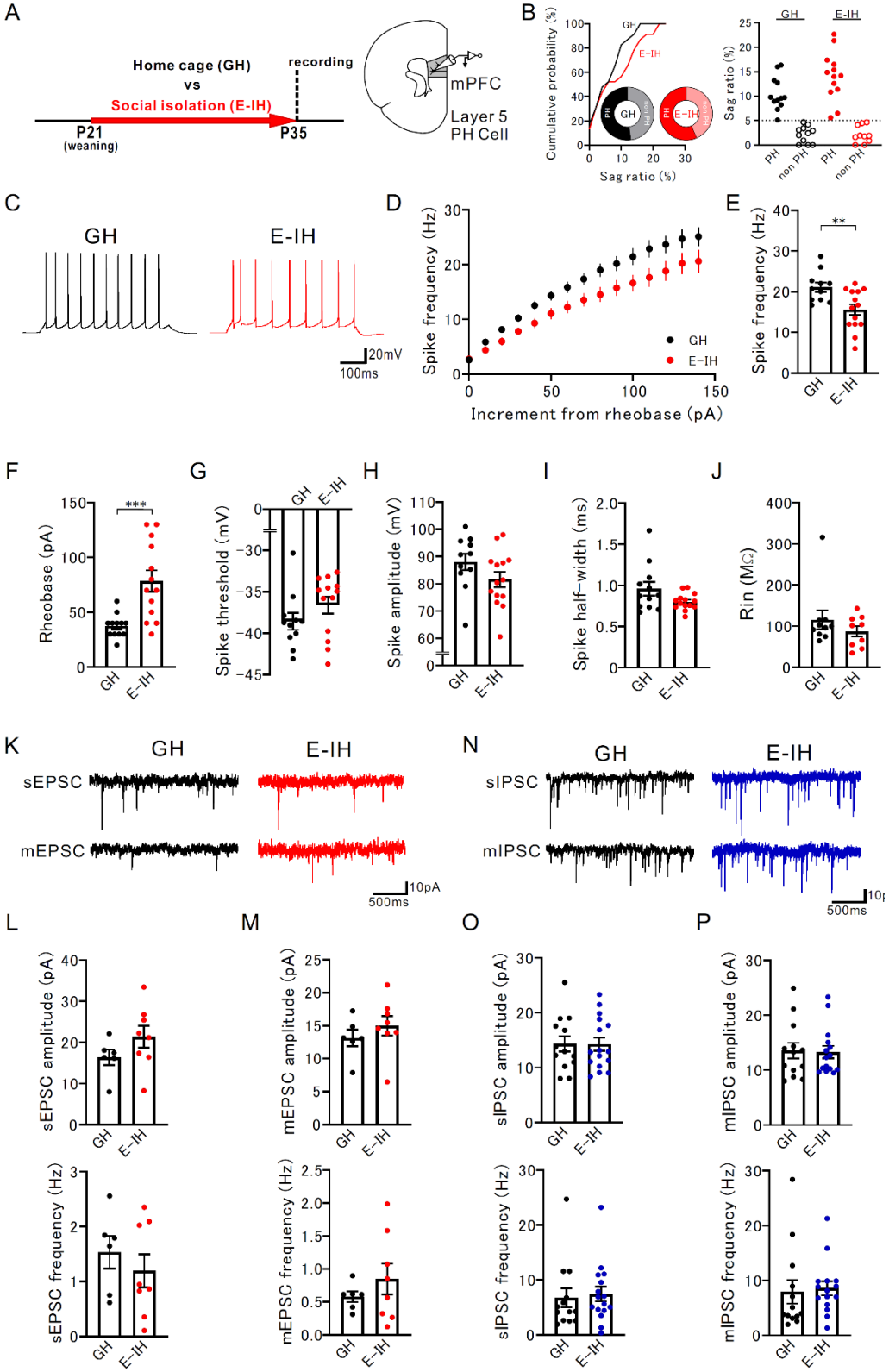

Figure 3.

(A) Left: experimental design of juvenile social isolation and recording at P35. Right: a

schema showing the whole-cell patch-clamp recording from L5 PH cells in the prelimbic cortex of GH and E-IH mice.

(B) Left: there was no difference in the cumulative probability of sag ratio of L5 pyramidal cell between GH and E-IH mice (Kolmogorov-Smirnov test, $P = 0.2372$, $n = 23$ (GH), 23 (E-IH)) and the pie chart showed the ratio of PH / non-PH cell in GH (n = 12 / 11) and E-IH (n = 13 / 10) mice. Right: the distribution of sag ratio of PH and non-PH in GH and E-IH mice.

(C) Representative spikes elicited by a current injection of 100-pA larger than the rheobase recorded from PH cells of GH mice (left) and E-IH mice (right) at P35.

(D) Frequency-current curves of the spikes of PH cells of GH mice (black) and E-IH mice (red) at P35.

(E) Juvenile social isolation reduced the spike frequency (two-tailed *t*-test, $t_{23} = 3.051$, $^{**}P = 0.0057$, $n = 11$ (GH), 14 (E-IH)).

(F) The rheobase of E-IH was significantly higher than that of GH (two-tailed *t*-test, $t_{23} = 3.880$, $^{***}P = 0.0008$, $n = 12$ (GH), 13 (E-IH)).

(G) There was no between-group difference in the spike threshold (Mann-Whitney *U* test, $U = 47$, $P = 0.1647$, $n = 11$ (GH), 13 (E-IH)).

(H) There was no between-group difference in the spike amplitude (two-tailed *t*-test, $t_{23} = 1.580$, $P = 0.1278$, $n = 11$ (GH), 14 (E-IH)).

(I) There was no between-group difference in the spike half-width (Mann-Whitney *U* test, $U = 55$, $P = 0.2200$, $n = 12$ (GH), 13 (E-IH)).

(J) There was no between-group difference in the input resistance (Mann-Whitney *U* test, $U = 41$, $P = 0.7802$, $n = 10$ (GH), 9 (E-IH)).

(K) Representative traces showing sEPSCs (top) and mEPSCs (bottom) recorded from PH cells in GH mice (left) and E-IH mice(right).

(L) There were no between-group differences in the sEPSC amplitude (top; two-tailed *t*-test, $t_{12} = 1.426$, $P = 0.1794$, $n = 6$ (GH), 8 (E-IH)), or sEPSC frequency (bottom; two-tailed *t*-test, $t_{12} = 0.7813$, $P = 0.4497$, $n = 6$ (GH), 8 (E-IH)).

(M) There were no between-group differences in the mEPSC amplitude (top; two-tailed *t*-test, $t_{12} = 0.9063$, $P = 0.3826$, $n = 6$ (GH), 8 (E-IH)), or mEPSC frequency (bottom; two-tailed *t*-test, $t_{12} = 0.9433$, $P = 0.3641$, $n = 6$ (GH), 8 (E-IH)).

(N) Representative traces showing sIPSCs (top) and mIPSCs (bottom) recorded from PH cells in GH mice (left) and E-IH mice(right).

(O) There were no between-group differences in the sIPSC amplitude (top; two-tailed *t*-test, $t_{27} = 0.03647$, $P = 0.9712$, $n = 13$ (GH), 16 (E-IH)), or sIPSC frequency (bottom; Mann-Whitney *U* test, $U = 84$, $P = 0.3983$, $n = 13$ (GH), 16 (E-IH)).

(P) There were no between-group differences in the mIPSC amplitude (top; Mann-Whitney *U* test, $U = 97$, $P > 0.9999$, $n = 13$ (GH), 15 (E-IH)), or mIPSC

frequency (bottom; Mann-Whitney *U* test, $U = 72.50$, $P = 0.2587$, $n = 13$ (GH), 15 (E-IH)).

***P < 0.001. Data are represented as means, and error bars indicate SEM.

The physiology of mPFC FSPV interneuron has already been affected immediately following social isolation.

We previously revealed that social isolation during the juvenile period altered the firing property and excitatory drive in mPFC L5 FSPV interneurons in adult mice (Yamamuro *et al.* 2020a). However, we do not know when these alterations in FSPV cells emerge as a result of juvenile social isolation. In the visual cortex, ocular deprivation alters the function of GABAergic interneurons, especially PVFS interneurons, prior to that of excitatory pyramidal cells (van Versendaal and Levelt 2016). Therefore, we hypothesized that by juvenile social isolation, the physiology of mPFC FSPV interneurons may change earlier than that of pyramidal cells. To investigate this possibility, we evaluated the physiological and morphological features of mPFC FSPV interneurons in GH and E-IH mice.

We first surveyed normal developmental changes in the morphological and physiological properties of FSPV interneurons. We confirmed that the GFP-positive cells in mPFC L5 in G42 mice were mostly coincident with PV-expressing cells by

immunostaining (Figure 4A) and that all recorded GFP-positive cells showed characteristic fast rhythmic firings in response to depolarizing current injection (Figure 4B and C) as shown previously (Chattopadhyaya *et al.* 2004; Yang et al. 2014). Biocytin-labeled FSPV cells have aspiny, beaded processes. Thick processes extending from the cell body exhibit periodic segmentation. Bifurcating thin processes consisted of oval nodes and interconnected rods. To examine the degree and orientation of dendritic ramification, we counted the number of processes passing through the cylindrical wall (height 20μm, diameter, 100μm) centering the cell body. Dendrites omnidirectionally arose from the soma. The orientation of dendritic extension from soma to the distal area was distributed evenly from 0° to 360°, which did not significantly differ from the uniform circular distribution (Kuiper's test, $p > 0.15$). The number of dendrites significantly decreased during development (Supplemental Figure 1A and B). Although neither the spike amplitude nor spike threshold changed, both spike frequency in response to depolarizing current injection and input resistance increased with development (Supplemental Figure 1C-F). These results are consistent with previous results for the developmental trajectories of PFC FSPV interneurons (Yang et al. 2018). However, both the sEPSC frequency and mEPSC frequency in FSPV cells significantly decreased with development (Supplemental Figure 2A-D). These results indicate that excitatory synaptic inputs to FSPV

interneurons decrease and, simultaneously, their intrinsic excitability increases from juvenile to adolescence in normal development with social experience.

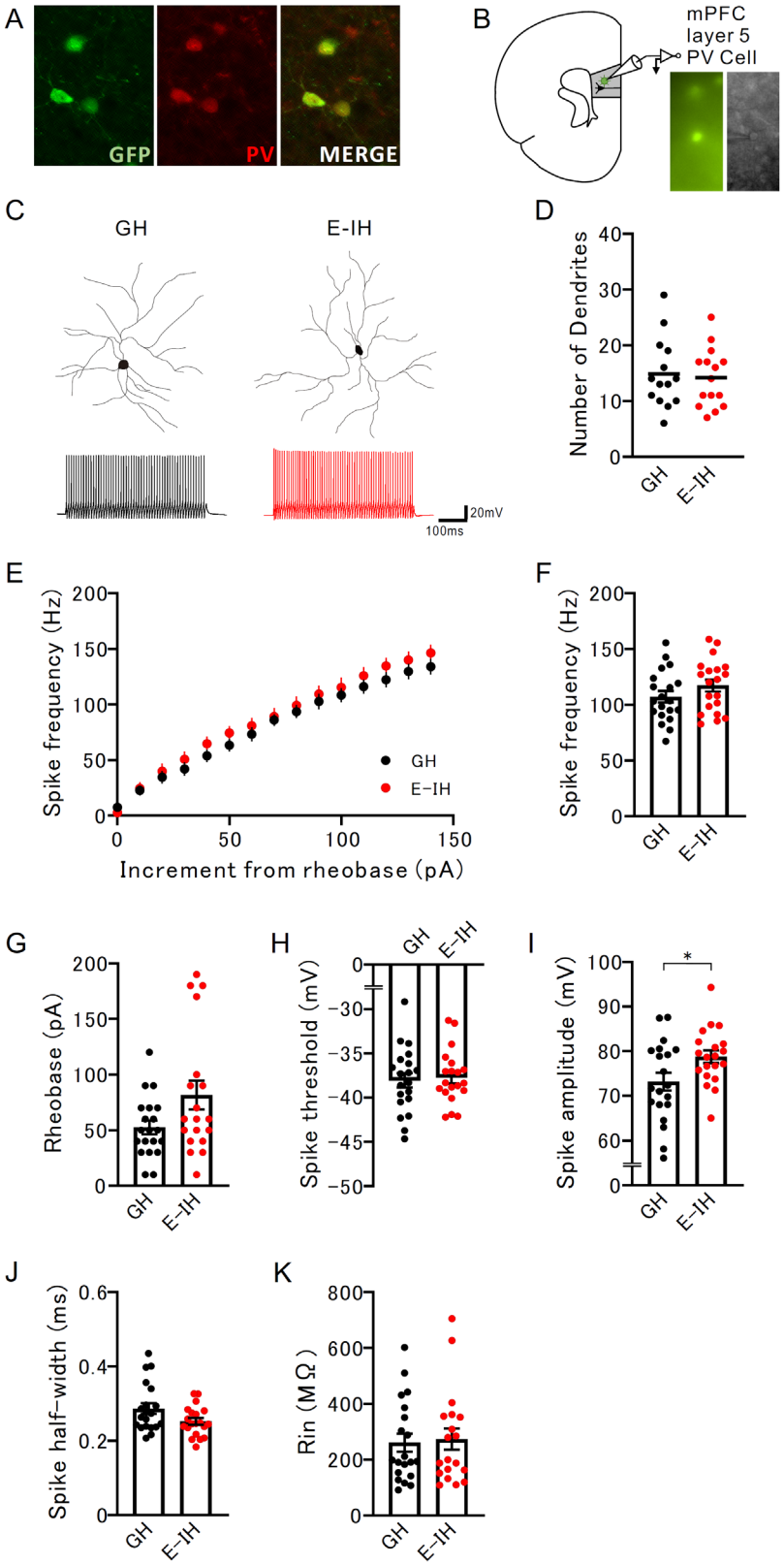
A
GFP
PV
MERGE
B
mPFC
layer 5
PV Cell
C
GH
E-IH
20mV
100ms
D
Number of Dendrites
GH
E-IH
E
Spike frequency (Hz)
Increment from rheobase (pA)
GH
E-IH
F
Spike frequency (Hz)
G
Rheobase (pA)
H
Spike threshold (mV)
I
Spike amplitude (mV)
*
J
Spike half-width (ms)
K
Rin (MΩ)

Figure 4

(A) Left: GFP expression in mPFC L5 of G42 mice. Middle: PV expression (red). Right: overlay of GFP and PV expression. Scale bars, 50 μ m.

(B) A schema showing the whole-cell patch-clamp recording from L5 PV cells labeled with GFP in the prelimbic cortex of GH and E-IH mice.

(C) Top: reconstruction of recorded PV cells of GH (left) and E-IH (right). Bottom: representative spikes elicited by a current injection of 100-pA lager than the rheobase recorded from PV cells of GH mice (left) and E-IH mice (right) at P35.

(D) There was no between-group difference in the number of dendrites (two-tailed *t*-test, t_{27} = 0.3375, *P* = 0.7384, *n* = 14 (GH), 15 (E-IH)).

(E) Frequency-current curves of the spikes of PV cells of GH mice (black) and E-IH mice (red) at P35.

(F) There were no between-group differences in the spike frequency (two-tailed *t*-test, t_{38} = 1.365, *P* = 0.1802, *n* = 20 (GH), 20 (E-IH)).

(G) There was no between-group difference in the rheobase (Mann-Whitney *U* test, *U* = 137, *P* = 0.1368, *n* = 20 (GH), 19 (E-IH)).

(H) There was no between-group difference in the spike threshold (two-tailed *t*-test, t_{38} = 0.3015, *P* = 0.7646, *n* = 20 (GH), 20 (E-IH)).

(I) Juvenile social isolation significantly increased the spike amplitude (two-tailed *t*-test, t_{38} = 2.303, **P* = 0.0268, *n* = 20 (GH), 20 (E-IH)).

(J) There was no between-group difference in the spike half-width (Mann-Whitney *U* test, $U = 144.5$, $P = 0.2061$, $n = 20$ (GH), 19 (E-IH)).

(K) There was no between-group difference in the input resistance (Mann-Whitney *U* test, $U = 188$, $P = 0.9611$, $n = 20$ (GH), 19 (E-IH)).

*$P < 0.05$. Data are represented as means and error bars indicate SEM.

Next, we compared the morphological and physiological properties of FSPV interneurons of E-IH mice to those of GH mice at P35 (Figure 4C-K). There was no significant difference in the number of dendrites between GH and E-IH mice (Figure 4D), indicating that juvenile social isolation had little effect on the morphological features of FSPV interneurons. Although there were no significant differences in the spike frequency (Figure 4F), rheobase (Figure 4G), spike threshold (Figure 4H), spike half-width (Figure 4J), or input resistance (Figure 4K), the spike amplitude in the E-IH group was larger than that in the GH group (Figure 4I). We then assessed the excitatory drive onto FSPV cells under normal conditions by applying no $GABA_A$ receptor blocker to the ACSF (Figure 5A and C). We observed that the sEPSC amplitude for FSPV cells in E-IH mice was significantly smaller than that in GH mice (Figure 5B). In contrast, the sEPSC frequency in FSPV cells in E-IH mice was significantly higher than that in GH mice (Figure 5B). Furthermore, we analyzed

mEPSCs, which represent the excitation-independent intrinsic activity of excitatory synapses. While there was no significant difference in the mEPSC amplitude, the mEPSC frequency in E-IH mice was significantly higher than that in GH mice (Figure 5D). These results indicate that excitatory synaptic inputs on FSPV interneurons are modified into small, but considerably frequent, inputs immediately after juvenile social isolation. Considering that the excitatory input onto PH pyramidal cells was unchanged immediately after social isolation, we suggest that juvenile social isolation preferentially affects FSPV interneurons, which are involved in inhibitory neuronal circuits, rather than PH pyramidal cells, in the early period.

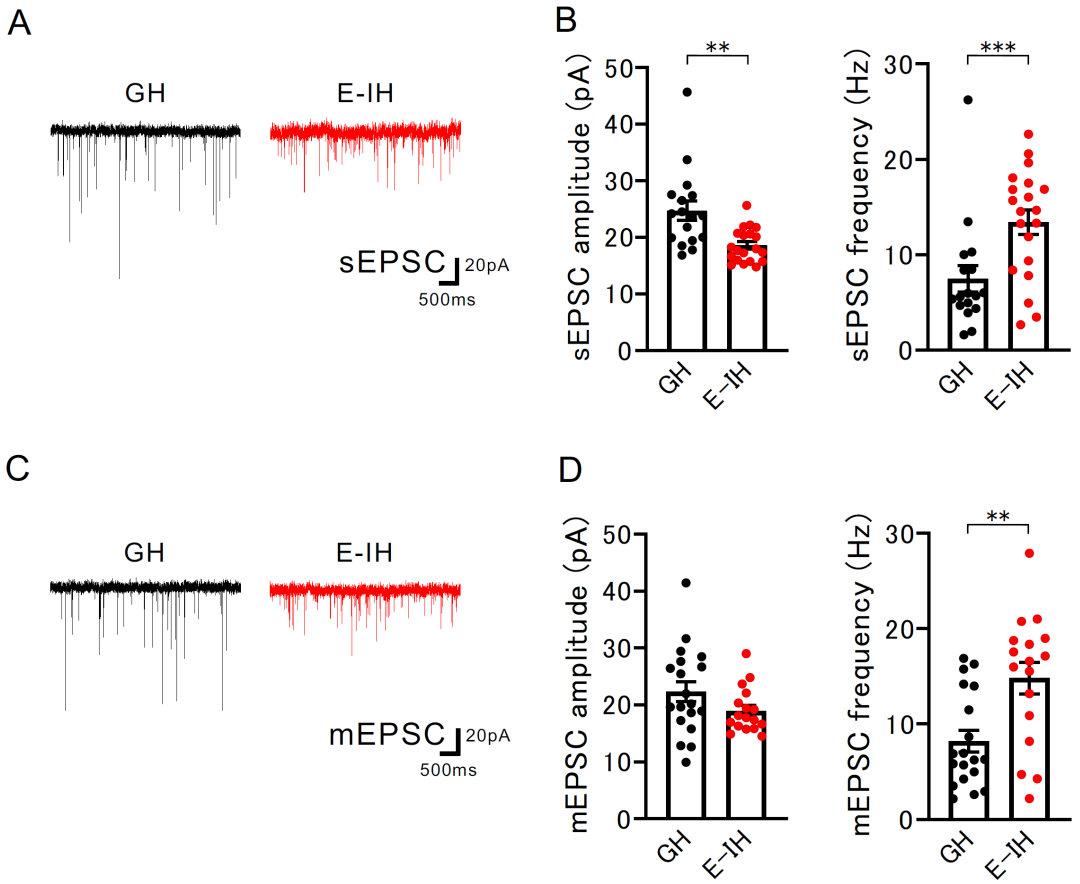

Figure 5

(A) Representative traces showing sEPSCs recorded from PV cells between GH (left) and E-IH (right).

(B) Left: sEPSC amplitude of E-IH mice was lower than that of GH mice (Mann-Whitney *U* test, $U = 62$, ***$P = 0.0007$, $n = 17$ (GH), 20 (E-IH)). Right: juvenile social isolation increased the sEPSC frequency significantly (Mann-Whitney *U* test, $U = 75$, **$P = 0.0031$, $n = 17$ (GH), 20 (E-IH)).

(C) Representative traces showing mEPSCs recorded from PV cells between GH (left) and E-IH (right).

(D) Left: there was no difference in mEPSC amplitude (Mann–Whitney *U* test, $U = 117$, $P = 0.1045$, $n = 19$ (GH), 18 (E-IH)). Right: juvenile social isolation increased the mEPSC frequency significantly (Mann-Whitney *U* test, $U = 77$, **$P = 0.0036$, $n = 19$ (GH), 18 (E-IH)).

**$P < 0.01$. ***$P < 0.001$. Data are represented as means and error bars indicate SEM.

Juvenile social isolation affects FSPV interneurons depending on subtype classified by the magnitude of h-current.

Neurons in the mammalian brain cortex are highly diverse and recently,

various types of neurons have been subdivided using various techniques (Klausberger and Somogyi 2008; Tremblay et al. 2016; Huang and Paul 2019), and interneurons are no exception. Gouwens et al. analyzed the correspondences among the morphological, electrophysiological, and transcriptomic features of GABAergic interneurons and developed an integrated classification for these interneurons in the primary visual cortex of mice (Gouwens et al. 2020). The authors subdivided FSPV interneurons into five subtypes, termed Pvalb-met 1–5. They reported that Pvalb-met types 1 to 3 were located in layer 5, in which we also recorded FSPV cells, and that the Pvalb-met 1 type of interneurons is characterized by a large h-current, which is recognized as the voltage sag in response to hyperpolarizing current injection. These characteristics may apply to other cortical areas, including agranular areas, such as the motor and prefrontal cortices. Furthermore, it is possible that each subtype of PV-expressing interneurons has a distinct functional role in the neuronal circuitry, and that social isolation may also have different effects on each subtype of PV-expressing interneurons. Therefore, we attempted to classify L5 FSPV interneurons using h-current features and examined the effect of juvenile social isolation on each subtype of L5 FSPV interneurons. However, there is the possibility that social isolation could affect the h-current itself in FSPV cells during this early period, which could invalidate the classification by h-current. We first examined

whether juvenile social isolation affects the distribution of the magnitude of h-current (sag ratio) of FSPV cells in both GH and E-IH mice. There was no significant difference in the distribution of the sag ratio between GH and E-IH at P35 (Figure 6A), indicating that juvenile social isolation has no effect on the h-current of FSPV interneurons. Next, we classified FSPV cells at P35 by the sag ratio; those with sag ratio 5% or more into “Type A cell” and those with sag ratio less than 5% into “Type B cell” (Figure 6A: Type A and Type B cell). We examined the intrinsic excitability and sEPSCs and mEPSCs of type A and B cells at P35 in GH mice reared in the normal environment and found no significant difference between the two types (Supplemental Figure 3). We then assessed the difference in both subtypes of FSPV cells between GH and E-IH at P35. Although we found no differences in morphology (Figure 6B and D) and input resistance (Figure 6C and E) between GH and E-IH in both Type A and Type B, surprisingly, both spike amplitude and spike frequency in response to depolarizing current injection for E-IH mice were significantly higher than those for GH mice only in type A cells, but not in type B cells (Figure 6F and G). However, excitatory synaptic inputs were similarly affected by juvenile social isolation in both subtypes: sEPSC amplitude was smaller, sEPSC frequency was higher, and mEPSC frequency was higher for E-IH than GH mice (Figure 6H and I). These results indicate that juvenile social isolation affected excitatory inputs to both types of FSPV

interneurons while it increased firing reactivity preferentially in type A cells.

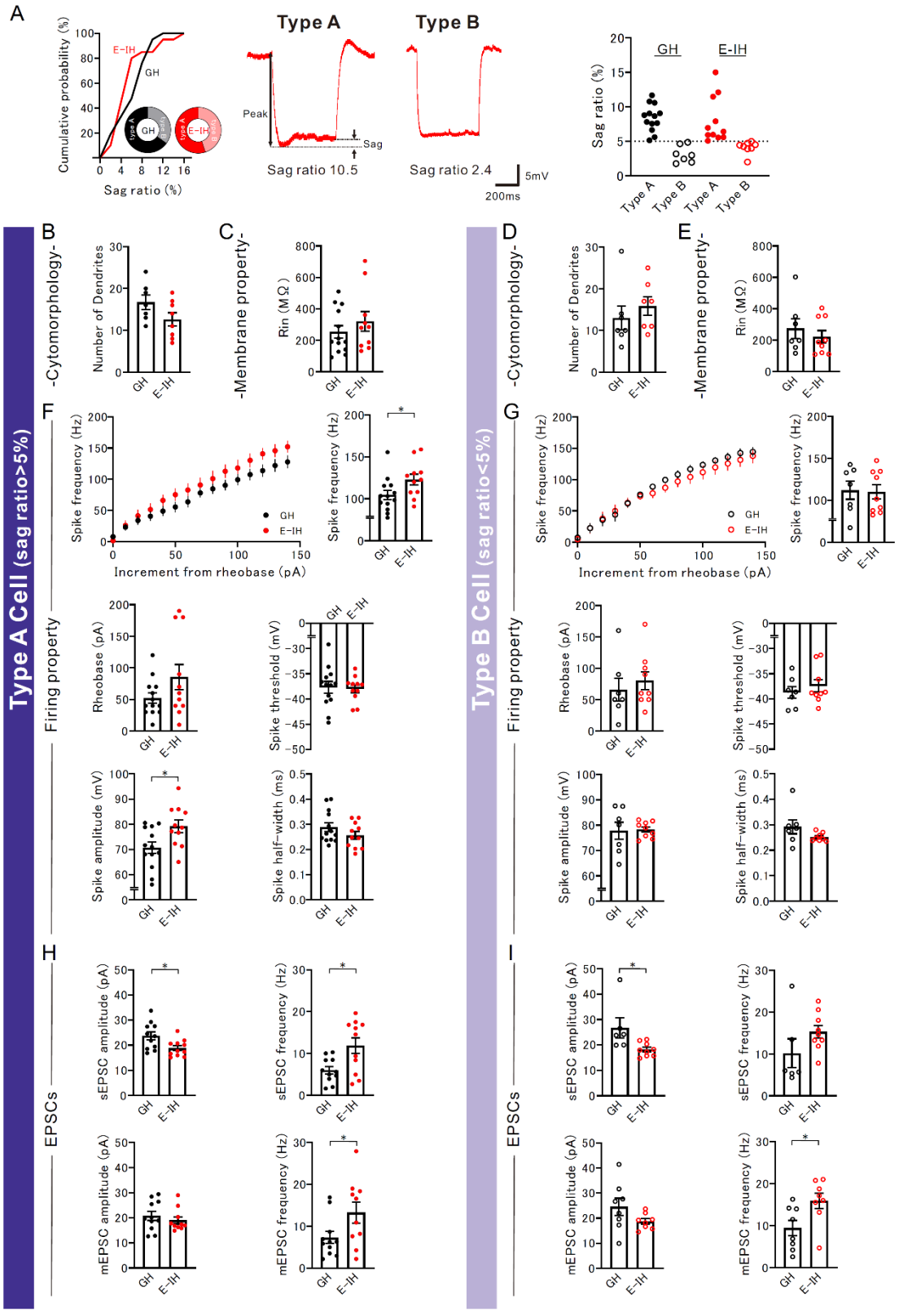

Figure 6

(A) Left: the cumulative distribution of sag ratio did not differ between GH and E-IH (Kolmogorov-Smirnov test, $P = 0.3878$) and the pie chart of type A / type B in GH (n = 13 / 7) and E-IH (n = 11 / 9) mice. Middle: type A cells with prominent voltage sag (> 5%) generated by a hyperpolarizing current injection (−50 pA, 500 ms). type B cells with slight voltage sag (< 5%). Sag ratio = 100* Sag / Peak. Right: the distribution of sag ratio of type A cells and type B cells in GH and E-IH mice.

(B and D) There were no significant differences in number of dendrites between GH and E-IH in either type A cell (left; two-tailed *t*-test, $t_{13} = 1.749$, $P = 0.1038$, $n = 7$ (GH), 8 (E-IH)) or type B cell (right; two-tailed *t*-test, $t_{12} = 0.7918$, $P = 0.4438$, $n = 7$ (GH), 7 (E-IH)).

(C and E) There were no significant differences in the input resistance between GH and E-IH in either type A cell (C: Mann-Whitney *U* test, $U = 54$, $P = 0.5224$, $n = 13$ (GH), 11 (E-IH)) or type B cell (E: two-tailed *t*-test, $t_{14} = 0.7336$, $P = 0.4753$, $n = 7$ (GH), 9 (E-IH)).

(F) Firing property of type A cells. Although there were no significant differences in the rheobase (Mann-Whitney *U* test, $U = 52.50$, $P = 0.2789$, $n = 13$ (GH), 11 (E-IH)), the spike threshold (two-tailed *t*-test, $t_{22} = 0.2075$, $P = 0.8376$, $n = 13$ (GH), 11 (E-IH)) or the spike half-width (Mann-Whitney *U* test, $U = 53$, $P = 0.2961$, $n = 13$ (GH), 11 (E-IH)), juvenile social isolation increased both of the spike frequency (two-tailed

t-test, t_{22} = 2.144, **P* = 0.0434, *n* = 13 (GH), 11 (E-IH)) and the spike amplitude (two-tailed *t*-test, t_{22} = 2.545, **P* = 0.0184, *n* = 13 (GH), 10 (E-IH)).

(G) Firing property of type B cells. There were no significant differences in the spike frequency (two-tailed *t*-test, t_{14} = 0.1313, *P* = 0.8974, *n* = 7 (GH), 9 (E-IH)), the rheobase (two-tailed *t*-test, t_{13} = 0.4437, *P* = 0.6645, *n* = 7 (GH), 8 (E-IH)), the spike threshold (two-tailed *t*-test, t_{14} = 0.7572, *P* = 0.4615, *n* = 7 (GH), 9 (E-IH)), the spike amplitude (two-tailed *t*-test, t_{14} = 0.1588, *P* = 0.8761, *n* = 7 (GH), 9 (E-IH)) or spike half-width (two-tailed *t*-test, t_{13} = 1.568, *P* = 0.1409, *n* = 7 (GH), 8 (E-IH)).

(H) EPSCs onto type A cells. The sEPSC amplitude of E-IH was lower than GH (two-tailed *t*-test, t_{20} = 2.545, **P* = 0.0193, *n* = 11 (GH), 11 (E-IH)). The sEPSC frequency of E-IH was higher than GH (two-tailed *t*-test, t_{20} = 2.813, **P* = 0.0107, *n* = 11 (GH), 11 (E-IH)). The mEPSC frequency of E-IH was also higher than GH (two-tailed *t*-test, t_{19} = 2.097, **P* = 0.0497, *n* = 11 (GH), 10 (E-IH)), but not the mEPSC amplitude (Mann-Whitney *U* test, *U* = 44, *P* = 0.4679, *n* = 11 (GH), 10 (E-IH)).

(I) EPSCs onto type B cells. The sEPSC amplitude of E-IH was lower than GH (two-tailed *t*-test, t_{13} = 2.532, **P* = 0.0250, *n* = 6 (GH), 9 (E-IH)). There were no significant differences in sEPSC frequency (two-tailed *t*-test, t_{13} = 1.527, *P* = 0.1507, *n* = 6 (GH), 9 (E-IH)). The mEPSC frequency of E-IH was higher than GH (two-tailed *t*-test, t_{14} = 2.476, **P* = 0.0267, *n* = 8 (GH), 8 (E-IH)), but not the mEPSC amplitude

(two-tailed *t*-test, $t_{14} = 1.634$, $P = 0.1246$, $n = 8$ (GH), 8 (E-IH)).

*$P < 0.05$. Data are represented as means and error bars indicate SEM.

Discussion

The mPFC pyramidal neurons project into subcortical areas, including the amygdala, nucleus accumbens (NAc), ventral tegmental area (VTA), and hypothalamus, which are important brain regions involved in social control (Ko 2017; Klune et al. 2021). Particularly, the axons of the cells with prominent h-current in mPFC L5 pyramidal neurons (PH pyramidal cells) project into the thalamus (Gee et al. 2012), pons (Dembrow et al. 2010), and amygdala (Ferreira et al. 2015; Avesar et al. 2018). In the present study, we surveyed normal developmental changes in firing properties of and excitatory inputs to PH pyramidal cells from weaning to adulthood (P21 to P65). We observed a decrease in spike threshold and an inclination of firing reactivity elevation with development after weaning, which is consistent with previous studies examining developmental changes for layer 5 cortical pyramidal cells in the visual cortex (Kasper et al. 1994) and PFC (Zhang 2004). We did not detect any quantitative changes in excitatory inputs to PH pyramidal cells. The number of histologically identified synapses in the mPFC decreases during adolescence after weaning, which is known as synapse pruning (Koss et al. 2014; Drzewiecki et al.

2016). It has been demonstrated that during adolescent development, synapses (synaptic spines) are not only lost but also newly generated and that the synapse turn-over by elimination and neogenesis plays a crucial role in rewiring neuronal circuits (Delevich et al. 2018). Our present results suggest that neogenesis and functionalization of excitatory synapses, as well as synapse pruning, concurrently occur to rebuild the neuronal circuit in a quantitatively balanced manner with post-weaning development.

According to an electrophysiological analysis of L5 pyramidal cells, we previously reported that juvenile social isolation eventually causes abnormalities in mPFC excitatory and inhibitory circuits in adult mice (Yamamuro *et al.* 2018; Yamamuro *et al.* 2020a). Abnormalities in adulthood can be summarized into two aspects: depressed activity in the excitatory circuit and excessive activity in the inhibitory circuit. The present results indicate that abnormalities in the circuit involving PH pyramidal cells belatedly emerged through the latent period. We also observed that juvenile social isolation caused no change in excitatory or inhibitory inputs to pyramidal neurons at the time point immediately after social isolation (P35). Additionally, at the early stage (P35), juvenile social isolation reduced the firing reactivity and increased the rheobase of PH pyramidal cells to depolarizing currents but maintained other properties of firing capacity at normal levels. This result could be

explained by an unbalanced development of voltage-dependent ion channels. Since the voltage threshold was unaffected by juvenile social isolation, the expression of voltage-dependent Na+ channels in E-IH mice may develop normally. One of the possibilities is that juvenile social isolation selectively facilitates the expression of voltage-dependent or calcium-dependent K+ channels. The over-expression of voltage-dependent or calcium-activated K+ channels could prohibit repetitive firings by their activation-induced outward current. Further, over-expression of slowly-inactivating K+ channels would reduce voltage response to depolarizing current and elevate the rheobase. Future studies investigating the normal development of ion channels and their changes caused by social isolation could determine the mechanism altering the firing capacity by social isolation. Meanwhile, we previously found that the intrinsic excitability and firing reactivity of PH pyramidal cells were reduced in adulthood (P65). This suggests that the firing capacity of pyramidal cells in PH gradually deteriorates from immediately after social isolation to adulthood. Our findings for PH pyramidal cells imply that the abnormalities of the circuit involving PH pyramidal cells may not be primary causal events, but are gradually induced by other mediating malfunctions. Similarly, Yamamuro et al. (Yamamuro et al. 2020b) reported that juvenile social isolation reduced the intrinsic excitability of medial prefrontal neurons projecting into the posterior paraventricular

thalamus (mPFC-pPVT) in adulthood but not at P35. Although no quantitative data for voltage sag to hyperpolarizing current have been presented, mPFC-pPVT pyramidal neurons seem to show apparent voltage sag, as evident from the representative data (Figure 5) reported by Yamamuro et al. (Yamamuro et al. 2020b). Therefore, the PH pyramidal cell population recorded in this study could have included mPFC-pPVT neurons. We need to investigate, more precisely, the interrelation between projection areas and electrophysiological properties of mPFC pyramidal neurons in the future.

In this study, we focused on the effect of juvenile social isolation on inhibitory and excitatory neuronal circuits at the early developmental stage (P35), two weeks after weaning. We observed that social isolation during the two weeks after weaning preferentially affected the function of FSPV interneurons, which are crucial devices for the mPFC inhibitory neuronal circuit. Our results also revealed that juvenile social isolation reduced the size but increased the frequency of excitatory synaptic inputs on FSPV interneurons. To interpret this result, it is necessary to refer to the normal development of FSPV interneurons. We found that excitatory inputs onto FSPV cells decreased in frequency and tended to increase in magnitude during 14 days period after weaning (P21 to P35). This may reflect the selection and pruning of excitatory synapses on FSPV interneurons in an activity-dependent manner during this period. It is already known that in the primate dorsolateral prefrontal cortex, some excitatory

synapses onto PV-expressing interneurons are pruned during adolescence, and the other residual synapses are potentiated (Donato et al. 2013; Chung et al. 2016; Chung et al. 2017). Previous evidence suggests that among many synapses converging on the same postsynaptic neuron, frequently activated synapses selectively survive, whereas rarely activated synapses are pruned (Yasuda et al. 2011). The pruning of synapses is thought to be mediated by JAK2 tyrosine kinase released from the presynaptic terminal as a “punishment signal” (Yasuda et al. 2021). The results of this study for EPSCs in mPFC FSPV interneurons are consistent with the picture on activity-dependent synapse refinement. In other words, although many excitatory inputs are randomly and diffusely connected to the inhibitory interneurons at weaning, some of the excitatory inputs may remain and be fully functionalized due to their adequate activities during adolescence, and other unnecessary synapses may be eliminated or defunctionalized. Importantly, it has been demonstrated that maternal immune activation inhibits synapse pruning in offspring mice, and unpruned synapses remain as-is to increase the EPSC frequency compared to normal mice (Andoh et al. 2019). This may have been the case in the present study. Juvenile social isolation may disturb the selection and pruning processes for circuit rebuilding and leave the inhibitory circuit in an immature state at weaning. The uneliminated excitatory inputs to FSPV interneurons may continue to work for a certain time, which

can enhance the activity of FSPV interneurons late in adolescence. Since our previous results revealed that juvenile social isolation causes a decrease in excitatory inputs on FSPV interneurons in adulthood (P65) (Yamamuro *et al.* 2020a), the social isolation-induced abounding excitatory synaptic inputs should be eliminated or defunctionalized before adulthood. However, this social isolation-induced excessive activation of FSPV interneurons can deteriorate the maturation of the excitatory circuit as well as alter the functional nature of the inhibitory circuit, even though it persists for a limited period. The electrophysiological data pertaining to mEPSC and sEPSC obtained in the present study by themselves do not fully prove that juvenile social isolation disturbs such activity-dependent synapse refinement. Future investigation using an elaborate technique such as enabling continual observation for excitatory synapses onto FSPV interneurons could provide definite evidence for this hypothesis.

In this study, we examined the possibility that juvenile social isolation has different effects on the subtypes of FSPV interneurons. We classified recorded FSPV interneurons into two types, A and B, based on the Ih magnitude. It is known that the magnitude of Ih for mPFC FSPV interneurons does not significantly change with age from adolescence to adulthood (Yang et al. 2018). Therefore, the classification in this study is not temporally applicable at a specific developmental stage but holds persistent validity from adolescence to adulthood. Our results indicate that this

classification is partially meaningful for the functional characterization of FSPV interneurons in the mPFC. We observed that juvenile social isolation enhanced firing reactivity and spike amplitude only in type A FSPV interneurons, whereas any effect of social isolation on firing properties was veiled in the overall analysis without the classification. The firing behavior of fast-spiking interneurons can be explained by the activities of three types of voltage-dependent ion channels: fast-activating/inactivating Na+, delayed rectifier K+ (Kv3.1–Kv3.2), and slowly-inactivating d-type K+ channels (Golomb et al. 2007). Among these three, voltage-dependent Na+ channels are almost the only determinant of the rising phase of the action potential. Since the spike threshold was not affected by juvenile social isolation even for type A FSPV interneurons, it is unlikely that juvenile social isolation causes the over-expression of voltage-dependent Na+ channels. Regarding cortical fast-spiking interneurons, the hyper-activity of delayed rectifier K+ channels has been shown to raise the firing frequency (Boddum et al. 2017). Thus, some modulation of delayed rectifier K+ channels could be related to the increased firing frequency caused by juvenile social isolation. Although this study showed that the firing capacity of FSPV interneurons increases with normal development for two weeks after weaning (Supplemental Figure 1), the detailed mechanism involved in this process should be clarified in a future study. Our result suggests that social isolation excessively promotes the

development of intrinsic firing capacity in a specific group of FSPV interneurons with prominent Ih. Ih is an inward current generated by the opening of hyperpolarization-activated cyclic nucleotide-gated (HCN) cation channels and is believed to facilitate re-excitation of neurons after hyperpolarization caused by excitation and/or inhibitory synaptic inputs. For excitatory neurons, Ih plays versatile and important roles, such as regulating excitability, controlling synaptic transmission, and initiating rhythmic firing (Huang et al. 2011; He et al. 2014; Gasselin et al. 2015). In particular, it has been demonstrated that blocking Ih suppresses oscillatory firing of hippocampal interneurons (Griguoli et al. 2010). Therefore, it is possible that type A FSPV interneurons are involved in the oscillatory activity of inhibitory circuitry, such as gamma-range oscillation (Sohal et al. 2009). Hyper-firing capacity induced by juvenile social isolation of type A FSPV interneurons could assist the impact of increased excitatory inputs onto FSPV cells to cause excessive activity of a specific population within the inhibitory circuit, at least for a certain period. In our previous study, we observed excessive inhibitory inputs to PH pyramidal cells in adulthood (Yamamuro *et al.* 2020a). Therefore, the social isolation that causes excessive activity of inhibitory circuits may belatedly emerge after early adolescence and persist until adulthood.

Neocortical GABAergic interneurons have been classified into distinct classes

based on their morphological, molecular, and physiological properties (Ascoli et al. 2008; DeFelipe et al. 2013). Among these, FSPV interneurons may have particularly important roles in adolescent neocortical development. Perineuronal nets (PNNs) are preferentially formed in the PV-positive interneurons of the primary visual cortex in an optical-experience-dependent manner during adolescence, which corresponds to the critical period for the functional development of the visual cortex (Ye and Miao 2013). More importantly, in the primary visual cortex, the change in excitatory input onto FSPV interneurons is involved in the experience-dependent modulation of visual responsiveness of excitatory pyramidal cells during the critical period (Kuhlman et al. 2013). Furthermore, the differentiation of hippocampal inhibitory neuronal circuity composed of FSPV interneurons is involved in experience-dependent behavioral modifications such as memory consolidation, retrieval, and learning and memory (Donato et al. 2013). These schemata that the activity of FSPV interneurons guides plastic modulation of the excitatory circuit inspire the following hypotheses about the role of mPFC FSPV interneurons in social-experience-dependent maturation of excitatory circuits in the mPFC. First, social experience during the two weeks after weaning promotes selection of suitable excitatory inputs onto mPFC FSPV interneurons and diminishes unnecessary and excessive excitatory inputs, which would control adequate actions by FSPV interneurons suppressing excitatory cell

activity. Second, the inhibitory circuit rebuilt through the first process releases some crucial activity of the excitatory circuit and guides activity-dependent rewiring of excitatory connections within the mPFC, as well as between the mPFC and other brain areas, which builds a mature mPFC neuronal circuit for cognitive and emotional functions. Our results support the hypothesis of the first process. As mentioned above, if the first process is disturbed, the resultant excessive activity of inhibitory interneurons would prohibit excitatory circuits from the activation-dependent building of synaptic connections between excitatory cells, which provides a possible explanation for our previous finding that social isolation causes a reduction in excitatory inputs to PH pyramidal cells in adulthood (Yamamuro et al. 2018). The reduced activity of excitatory cells would adversely reduce the functional excitatory synapses onto inhibitory interneurons in an activation-dependent manner, which is consistent with previous findings (Yamamuro et al. 2018). Although our present result that the social isolation-caused alterations of excitatory circuits remain latent immediately after social isolation can be explained by our hypothesis on the second developmental process, we cannot provide any determinate proof at present. It is necessary to investigate the role of mPFC FSPV interneurons in guiding the experience-dependent modulation of excitatory circuitry during developmental periods in the future. In addition, an important question of how the activation of

neurons modulates their intrinsic firing properties during the developmental period remains unsolved, although our findings suggest that the activation of FSPV interneurons raises its firing capacity, at least for a specific subpopulation. This suggests that type A and type B FSPV interneurons are functionally different populations, possibly, the so-called specialist and generalist ones. Type A FSPV interneurons might be destined to respond to a specific pattern of excitatory inputs and to inhibit a qualified pyramidal cell population related to the development of social cognition and behavior. Due to the frequent but small excitatory inputs caused by juvenile social isolation, type A FSPV interneurons accommodate to detect and respond to a tiny input change buried in abundant inputs, which would be observed as hyperfiring reactivity. Conversely, type B FSPV interneurons might be involved in maintaining a general excitation-inhibition balance, which could be executed by responding to the total amount of inputs. Since this schema is still a tentative and unfounded speculation, in the future, we should investigate how FSPV interneurons can be differentiated functionally, morphologically, and molecularly before determining why the firing capacity of type A FSPV is preferentially affected by social isolation. The classification based on this electrophysiological property alone may be a tentative one at present. To definitely identify a specific cell population, transcriptomic approaches, such as patch-seq, should be applied.

In a previous study (Bick et al. 2020), juvenile social isolation did not affect PV-positive interneurons in terms of excitatory inputs or firing reactivity to depolarizing current injections at P35 immediately after social isolation. On the other hand, we detected definite alterations in excitatory inputs on FSPV interneurons at P35. This discrepancy could arise from the incongruity in FSPV interneuron populations investigated between the two studies. We analyzed FSPV interneurons located in layer 5 of prelimbic and infralimbic areas. The dorsal-medial PFC, in which Bicks et al. recorded the presence of FSPV interneurons, consists of the most anterior part of the cingulate and prelimbic cortices. Although the two recorded FSPV interneuron populations appear to overlap with each other in the prelimbic cortex, a considerable part of the FSPV interneuron population recorded in this study appears to be excluded from the analysis in the study by Bicks et al. In addition, although we did not detect any alteration in firing capacity by juvenile social isolation, we found an enhancing effect on firing reactivity only for a specific subpopulation of FSPV interneurons. This suggests that juvenile social isolation may or may not differentially affect some subclasses of FSPV interneurons. Each subtype of FSPV interneurons may be eccentrically distributed in infralimbic, prelimbic, and anterior cingulate areas. The classification of FSPV interneurons based on their histological and functional properties is necessary to assess the effects of juvenile social isolation on the

developmental processes of FSPV interneurons. Another possible reason for this discrepancy is the difference in mouse genetics. We used G42 mice, and Bick et al. 2020 used PV-Cre mice. However, at present, we cannot propose any logical explanation of how this genetic difference in mice could relate to the differential natures of FSPV interneurons.

This study has some other limitations. We used isoflurane anesthesia in mice during the slice preparation. Isoflurane affects neuronal transmission and excitability in brain neurons (Peters et al. 2008; Zhao et al. 2019; Guo et al. 2021). If these effects of isoflurane persist for more than one hour after incubation, our observations could have been influenced by the effects of isoflurane. We cannot completely exclude the possibility that social isolation can modify the sensitivity to isoflurane. Another limitation that should be addressed in the future is the ambiguity in the source of excitatory input on FSPV interneurons. We found alterations in excitatory inputs on FSPV interneurons by social isolation. However, the excitatory input from which FSPV interneurons are influenced remains unclear. L5 FSPV interneurons receive strong intralaminar (horizontal) excitatory inputs from L5 pyramidal cells and moderate interlaminar (vertical) excitatory inputs from L2/3 pyramidal cells (Otsuka and Kawaguchi 2009; Apicella et al. 2012; Naka and Adesnik 2016; Morishima et al. 2017). Therefore, juvenile social isolation could affect either of the two sources of

pyramidal cell populations. In addition, whether alterations in mEPSCs and sEPSCs induced by social isolation correspond to some aberrations in functional synaptic transmission should be determined because the change in miniature EPSC does not always correspond with that in evoked EPSC (Capogna et al. 1996). To resolve these questions, a prospective analysis of unitary EPSCs and IPSCs with paired recordings between FSPV interneurons and L5 (PH / non-PH) or L2/3 pyramidal cells, which could reveal detailed changes in synaptic function induced by social isolation, should be performed. We showed that juvenile social isolation affected excitatory synaptic inputs on FSPV interneurons but not on PH cells at P35. However, we cannot exclude the possibility that we failed to detect the effect of PH cells by social isolation on distal apical dendrites due to space clamp error (Williams and Mitchell 2008). In conclusion, our findings revealed a subtype of PV cells with high h-currents that are preferentially affected at the early stage of social isolation. Abnormalities in neural circuitry during the early development of social isolation have not been identified previously. Thus, this is the first such report and our findings may shed light on understanding the mechanisms underlying social experience and neurodevelopment.

Funding

This work was supported by JSPS KAKENHI;, Grant Numbers JP19K17117

and JP 19K08078.

Acknowledgments

We would like to thank the members of the Department of Neurophysiology, Nara Medical University, for assisting with electrophysiological experiments. And, we would like to thank Editage (www.editage.com) for English language editing.

Author contributions

K.O. and H. Y. designed and analyzed the experiments and wrote the manuscript with input from all authors. K.O. performed most experiments in part assisted by K.Y., Y.N., and Y.O. Immunohistochemistry was assisted by Y.O., Y.Y., M.I., and S.K., and H.Y., Y.S., and T.K. supervised the experiments.

References

Agrawal HC, Fox MW, Himwich WA. 1967. Neurochemical and behavioral effects of isolation-rearing in the dog. Life Sci. 6:71-78.

Andoh M, Shibata K, Okamoto K, Onodera J, Morishita K, Miura Y, Ikegaya Y, Koyama R. 2019. Exercise Reverses Behavioral and Synaptic Abnormalities after Maternal Inflammation. Cell Rep. 27:2817-2825.e2815.

Apicella AJ, Wickersham IR, Seung HS, Shepherd GM. 2012. Laminarly orthogonal excitation of fast-spiking and low-threshold-spiking interneurons in mouse motor cortex. J Neurosci. 32:7021-7033.

Arnsten AF, Rubia K. 2012. Neurobiological circuits regulating attention, cognitive control, motivation, and emotion: disruptions in neurodevelopmental psychiatric disorders. J Am Acad Child Adolesc Psychiatry. 51:356-367.

Ascoli GA, Alonso-Nanclares L, Anderson SA, Barrionuevo G, Benavides-Piccione R, Burkhalter A, Buzsáki G, Cauli B, Defelipe J, Fairén A, Feldmeyer D, Fishell G, Fregnac Y, Freund TF, Gardner D, Gardner EP, Goldberg JH, Helmstaedter M, Hestrin S, Karube F, Kisvárday ZF, Lambolez B, Lewis DA, Marin O, Markram H, Muñoz A, Packer A, Petersen CC, Rockland KS, Rossier J, Rudy B, Somogyi P, Staiger JF, Tamas G, Thomson AM, Toledo-Rodriguez M, Wang Y, West DC, Yuste R. 2008. Petilla terminology: nomenclature of features of GABAergic interneurons of the cerebral cortex. Nat Rev Neurosci. 9:557-568.

Avesar D, Stephens EK, Gulledge AT. 2018. Serotonergic Regulation of Corticoamygdalar Neurons in the Mouse Prelimbic Cortex. Front Neural Circuits. 12:63.

Bicks LK, Yamamuro K, Flanigan ME, Kim JM, Kato D, Lucas EK, Koike H, Peng MS, Brady DM, Chandrasekaran S, Norman KJ, Smith MR, Clem RL, Russo SJ, Akbarian

S, Morishita H. 2020. Prefrontal parvalbumin interneurons require juvenile social experience to establish adult social behavior. Nat Commun 11:1003.

Boddum K, Hougaard C, Xiao-Ying Lin J, von Schoubye NL, Jensen HS, Grunnet M, Jespersen T. 2017. K(v)3.1/K(v)3.2 channel positive modulators enable faster activating kinetics and increase firing frequency in fast-spiking GABAergic interneurons. Neuropharmacology. 118:102-112.

Bos K, Zeanah CH, Fox NA, Drury SS, McLaughlin KA, Nelson CA. 2011. Psychiatric outcomes in young children with a history of institutionalization. Harv Rev Psychiatry. 19:15-24.

Capogna M, Gähwiler BH, Thompson SM. 1996. Calcium-independent actions of alpha-latrotoxin on spontaneous and evoked synaptic transmission in the hippocampus. J Neurophysiol. 76:3149-3158.

Chattopadhyaya B, Di Cristo G, Higashiyama H, Knott GW, Kuhlman SJ, Welker E, Huang ZJ. 2004. Experience and activity-dependent maturation of perisomatic GABAergic innervation in primary visual cortex during a postnatal critical period. J Neurosci. 24:9598-9611.

Chugani HT, Behen ME, Muzik O, Juhász C, Nagy F, Chugani DC. 2001. Local brain functional activity following early deprivation: a study of postinstitutionalized Romanian orphans. Neuroimage. 14:1290-1301.

Chung DW, Fish KN, Lewis DA. 2016. Pathological Basis for Deficient Excitatory Drive to Cortical Parvalbumin Interneurons in Schizophrenia. Am J Psychiatry. 173:1131-1139.

Chung DW, Wills ZP, Fish KN, Lewis DA. 2017. Developmental pruning of excitatory synaptic inputs to parvalbumin interneurons in monkey prefrontal cortex. Proc Natl Acad Sci U S A. 114:E629-e637.

Dalley JW, Cardinal RN, Robbins TW. 2004. Prefrontal executive and cognitive functions in rodents: neural and neurochemical substrates. Neurosci Biobehav Rev. 28:771-784.

DeFelipe J, López-Cruz PL, Benavides-Piccione R, Bielza C, Larrañaga P, Anderson S, Burkhalter A, Cauli B, Fairén A, Feldmeyer D, Fishell G, Fitzpatrick D, Freund TF, González-Burgos G, Hestrin S, Hill S, Hof PR, Huang J, Jones EG, Kawaguchi Y, Kisvárday Z, Kubota Y, Lewis DA, Marín O, Markram H, McBain CJ, Meyer HS, Monyer H, Nelson SB, Rockland K, Rossier J, Rubenstein JL, Rudy B, Scanziani M, Shepherd GM, Sherwood CC, Staiger JF, Tamás G, Thomson A, Wang Y, Yuste R, Ascoli GA. 2013. New insights into the classification and nomenclature of cortical GABAergic interneurons. Nat Rev Neurosci. 14:202-216.

Delevich K, Thomas AW, Wilbrecht L. 2018. Adolescence and "Late Blooming" Synapses of the Prefrontal Cortex. Cold Spring Harb Symp Quant Biol. 83:37-43.

Dembrow NC, Chitwood RA, Johnston D. 2010. Projection-specific neuromodulation of medial prefrontal cortex neurons. J Neurosci. 30:16922-16937.

Dienel SJ, Lewis DA. 2019. Alterations in cortical interneurons and cognitive function in schizophrenia. Neurobiol Dis. 131:104208.

Donato F, Rompani SB, Caroni P. 2013. Parvalbumin-expressing basket-cell network plasticity induced by experience regulates adult learning. Nature. 504:272-276.

Drzewiecki CM, Willing J, Juraska JM. 2016. Synaptic number changes in the medial prefrontal cortex across adolescence in male and female rats: A role for pubertal onset. Synapse. 70:361-368.

Egeland B, Sroufe LA, Erickson M. 1983. The developmental consequence of different patterns of maltreatment. Child Abuse Negl. 7:459-469.

Eluvathingal TJ, Chugani HT, Behen ME, Juhász C, Muzik O, Maqbool M, Chugani DC, Makki M. 2006. Abnormal brain connectivity in children after early severe socioemotional deprivation: a diffusion tensor imaging study. Pediatrics. 117:2093-2100.

Endo N, Ujita W, Fujiwara M, Miyauchi H, Mishima H, Makino Y, Hashimoto L, Oyama H, Makinodan M, Nishi M, Tohyama C, Kakeyama M. 2018. Multiple animal positioning system shows that socially-reared mice influence the social proximity of isolation-reared cagemates. Commun Biol. 1:225.

Ferreira AN, Yousuf H, Dalton S, Sheets PL. 2015. Highly differentiated cellular and circuit properties of infralimbic pyramidal neurons projecting to the periaqueductal gray and amygdala. Front Cell Neurosci. 9:161.

Gasselin C, Inglebert Y, Debanne D. 2015. Homeostatic regulation of h-conductance controls intrinsic excitability and stabilizes the threshold for synaptic modification in CA1 neurons. J Physiol. 593:4855-4869.

Gee S, Ellwood I, Patel T, Luongo F, Deisseroth K, Sohal VS. 2012. Synaptic activity unmasks dopamine D2 receptor modulation of a specific class of layer V pyramidal neurons in prefrontal cortex. J Neurosci. 32:4959-4971.

Golomb D, Donner K, Shacham L, Shlosberg D, Amitai Y, Hansel D. 2007. Mechanisms of firing patterns in fast-spiking cortical interneurons. PLoS Comput Biol. 3:e156.

Gonchar Y, Wang Q, Burkhalter A. 2007. Multiple distinct subtypes of GABAergic neurons in mouse visual cortex identified by triple immunostaining. Front Neuroanat. 1:3.

Gouwens NW, Sorensen SA, Baftizadeh F, Budzillo A, Lee BR, Jarsky T, Alfiler L, Baker K, Barkan E, Berry K, Bertagnolli D, Bickley K, Bomben J, Braun T, Brouner K, Casper T, Crichton K, Daigle TL, Dalley R, de Frates RA, Dee N, Desta T, Lee SD, Dotson N, Egdorf T, Ellingwood L, Enstrom R, Esposito L, Farrell C, Feng D, Fong O,

Gala R, Gamlin C, Gary A, Glandon A, Goldy J, Gorham M, Graybuck L, Gu H, Hadley K, Hawrylycz MJ, Henry AM, Hill D, Hupp M, Kebede S, Kim TK, Kim L, Kroll M, Lee C, Link KE, Mallory M, Mann R, Maxwell M, McGraw M, McMillen D, Mukora A, Ng L, Ng L, Ngo K, Nicovich PR, Oldre A, Park D, Peng H, Penn O, Pham T, Pom A, Popović Z, Potekhina L, Rajanbabu R, Ransford S, Reid D, Rimorin C, Robertson M, Ronellenfitch K, Ruiz A, Sandman D, Smith K, Sulc J, Sunkin SM, Szafer A, Tieu M, Torkelson A, Trinh J, Tung H, Wakeman W, Ward K, Williams G, Zhou Z, Ting JT, Arkhipov A, Sümbül U, Lein ES, Koch C, Yao Z, Tasic B, Berg J, Murphy GJ, Zeng H. 2020. Integrated Morphoelectric and Transcriptomic Classification of Cortical GABAergic Cells. Cell. 183:935-953.e919.

Griguoli M, Maul A, Nguyen C, Giorgetti A, Carloni P, Cherubini E. 2010. Nicotine blocks the hyperpolarization-activated current Ih and severely impairs the oscillatory behavior of oriens-lacunosum moleculare interneurons. J Neurosci. 30:10773-10783.

Guo J, Ran M, Gao Z, Zhang X, Wang D, Li H, Zhao S, Sun W, Dong H, Hu J. 2021. Cell-type-specific imaging of neurotransmission reveals a disrupted excitatory-inhibitory cortical network in isoflurane anaesthesia. EBioMedicine. 65:103272.

Hare BD, Duman RS. 2020. Prefrontal cortex circuits in depression and anxiety: contribution of discrete neuronal populations and target regions. Mol Psychiatry.

25:2742-2758.

Harlow HF, Dodsworth RO, Harlow MK. 1965. Total social isolation in monkeys. Proc Natl Acad Sci U S A. 54:90-97.

He C, Chen F, Li B, Hu Z. 2014. Neurophysiology of HCN channels: from cellular functions to multiple regulations. Prog Neurobiol. 112:1-23.

Huang Z, Lujan R, Kadurin I, Uebele VN, Renger JJ, Dolphin AC, Shah MM. 2011. Presynaptic HCN1 channels regulate Cav3.2 activity and neurotransmission at select cortical synapses. Nat Neurosci. 14:478-486.

Huang ZJ, Paul A. 2019. The diversity of GABAergic neurons and neural communication elements. Nat Rev Neurosci. 20:563-572.

Kasper EM, Lübke J, Larkman AU, Blakemore C. 1994. Pyramidal neurons in layer 5 of the rat visual cortex. III. Differential maturation of axon targeting, dendritic morphology, and electrophysiological properties. J Comp Neurol. 339:495-518.

Kawaguchi Y, Otsuka T, Morishima M, Ushimaru M, Kubota Y. 2019. Control of excitatory hierarchical circuits by parvalbumin-FS basket cells in layer 5 of the frontal cortex: insights for cortical oscillations. J Neurophysiol. 121:2222-2236.

Ke MT, Nakai Y, Fujimoto S, Takayama R, Yoshida S, Kitajima TS, Sato M, Imai T. 2016. Super-Resolution Mapping of Neuronal Circuitry With an Index-Optimized Clearing Agent. Cell Rep. 14:2718-2732.

Klausberger T, Somogyi P. 2008. Neuronal diversity and temporal dynamics: the unity of hippocampal circuit operations. Science. 321:53-57.

Klune CB, Jin B, DeNardo LA. 2021. Linking mPFC circuit maturation to the developmental regulation of emotional memory and cognitive flexibility. Elife. 10.

Ko J. 2017. Neuroanatomical Substrates of Rodent Social Behavior: The Medial Prefrontal Cortex and Its Projection Patterns. Frontiers in Neural Circuits. 11.

Kolb B, Mychasiuk R, Muhammad A, Li Y, Frost DO, Gibb R. 2012. Experience and the developing prefrontal cortex. Proc Natl Acad Sci U S A. 109 Suppl 2:17186-17193.

Koss WA, Belden CE, Hristov AD, Juraska JM. 2014. Dendritic remodeling in the adolescent medial prefrontal cortex and the basolateral amygdala of male and female rats. Synapse. 68:61-72.

Kuhlman SJ, Olivas ND, Tring E, Ikrar T, Xu X, Trachtenberg JT. 2013. A disinhibitory microcircuit initiates critical-period plasticity in the visual cortex. Nature. 501:543-546.

Lee AT, Gee SM, Vogt D, Patel T, Rubenstein JL, Sohal VS. 2014. Pyramidal neurons in prefrontal cortex receive subtype-specific forms of excitation and inhibition. Neuron. 81:61-68.

Makinodan M, Rosen KM, Ito S, Corfas G. 2012. A critical period for social experience-dependent oligodendrocyte maturation and myelination. Science.

337:1357-1360.

Markram H, Toledo-Rodriguez M, Wang Y, Gupta A, Silberberg G, Wu C. 2004. Interneurons of the neocortical inhibitory system. Nat Rev Neurosci. 5:793-807.

McCormick DA, Prince DA. 1987. Post-natal development of electrophysiological properties of rat cerebral cortical pyramidal neurones. J Physiol. 393:743-762.

Miller EK, Cohen JD. 2001. An integrative theory of prefrontal cortex function. Annu Rev Neurosci. 24:167-202.

Morishima M, Kawaguchi Y. 2006. Recurrent connection patterns of corticostriatal pyramidal cells in frontal cortex. J Neurosci. 26:4394-4405.

Morishima M, Kobayashi K, Kato S, Kobayashi K, Kawaguchi Y. 2017. Segregated Excitatory-Inhibitory Recurrent Subnetworks in Layer 5 of the Rat Frontal Cortex. Cereb Cortex. 27:5846-5857.

Naka A, Adesnik H. 2016. Inhibitory Circuits in Cortical Layer 5. Frontiers in Neural Circuits. 10.

Neher E. 1992. Correction for liquid junction potentials in patch clamp experiments. Methods Enzymol. 207:123-131.

Otsuka T, Kawaguchi Y. 2009. Cortical inhibitory cell types differentially form intralaminar and interlaminar subnetworks with excitatory neurons. J Neurosci. 29:10533-10540.

Peters JH, McDougall SJ, Mendelowitz D, Koop DR, Andresen MC. 2008. Isoflurane differentially modulates inhibitory and excitatory synaptic transmission to the solitary tract nucleus. Anesthesiology. 108:675-683.

Pollak SD, Nelson CA, Schlaak MF, Roeber BJ, Wewerka SS, Wiik KL, Frenn KA, Loman MM, Gunnar MR. 2010. Neurodevelopmental effects of early deprivation in postinstitutionalized children. Child Dev. 81:224-236.

Rudy B, Fishell G, Lee S, Hjerling-Leffler J. 2011. Three groups of interneurons account for nearly 100% of neocortical GABAergic neurons. Dev Neurobiol. 71:45-61.

Sohal VS, Zhang F, Yizhar O, Deisseroth K. 2009. Parvalbumin neurons and gamma rhythms enhance cortical circuit performance. Nature. 459:698-702.

Tremblay R, Lee S, Rudy B. 2016. GABAergic Interneurons in the Neocortex: From Cellular Properties to Circuits. Neuron. 91:260-292.

van Versendaal D, Levelt CN. 2016. Inhibitory interneurons in visual cortical plasticity. Cell Mol Life Sci. 73:3677-3691.

Williams SR, Mitchell SJ. 2008. Direct measurement of somatic voltage clamp errors in central neurons. Nat Neurosci. 11:790-798.

Wood JN, Romero SG, Makale M, Grafman J. 2003. Category-specific representations of social and nonsocial knowledge in the human prefrontal cortex. J Cogn Neurosci. 15:236-248.

Xu P, Chen A, Li Y, Xing X, Lu H. 2019. Medial prefrontal cortex in neurological diseases. Physiol Genomics. 51:432-442.

Xu X, Roby KD, Callaway EM. 2010. Immunochemical characterization of inhibitory mouse cortical neurons: three chemically distinct classes of inhibitory cells. J Comp Neurol. 518:389-404.

Yamamuro K, Bicks LK, Leventhal MB, Kato D, Im S, Flanigan ME, Garkun Y, Norman KJ, Caro K, Sadahiro M, Kullander K, Akbarian S, Russo SJ, Morishita H. 2020b. A prefrontal-paraventricular thalamus circuit requires juvenile social experience to regulate adult sociability in mice. Nat Neurosci 23:1240-1252.

Yamamuro K, Yoshino H, Ogawa Y, Makinodan M, Toritsuka M, Yamashita M, Corfas G, Kishimoto T. 2018. Social Isolation During the Critical Period Reduces Synaptic and Intrinsic Excitability of a Subtype of Pyramidal Cell in Mouse Prefrontal Cortex. Cereb Cortex. 28:998-1010.

Yamamuro K, Yoshino H, Ogawa Y, Okamura K, Nishihata Y, Makinodan M, Saito Y, Kishimoto T. 2020a. Juvenile Social Isolation Enhances the Activity of Inhibitory Neuronal Circuits in the Medial Prefrontal Cortex. Front Cell Neurosci. 14:105.

Yang JM, Zhang J, Yu YQ, Duan S, Li XM. 2014. Postnatal development of 2 microcircuits involving fast-spiking interneurons in the mouse prefrontal cortex. Cereb Cortex. 24:98-109.

Yang SS, Li YC, Coley AA, Chamberlin LA, Yu P, Gao WJ. 2018. Cell-Type Specific Development of the Hyperpolarization-Activated Current, Ih, in Prefrontal Cortical Neurons. Front Synaptic Neurosci. 10:7.

Yasuda M, Johnson-Venkatesh EM, Zhang H, Parent JM, Sutton MA, Umemori H. 2011. Multiple forms of activity-dependent competition refine hippocampal circuits in vivo. Neuron. 70:1128-1142.

Yasuda M, Nagappan-Chettiar S, Johnson-Venkatesh EM, Umemori H. 2021. An activity-dependent determinant of synapse elimination in the mammalian brain. Neuron. 109:1333-1349.e1336.

Ye Q, Miao QL. 2013. Experience-dependent development of perineuronal nets and chondroitin sulfate proteoglycan receptors in mouse visual cortex. Matrix Biol. 32:352-363.

Zhang ZW. 2004. Maturation of layer V pyramidal neurons in the rat prefrontal cortex: intrinsic properties and synaptic function. J Neurophysiol. 91:1171-1182.

Zhao W, Zhang M, Liu J, Liang P, Wang R, Hemmings HC, Zhou C. 2019. Isoflurane Modulates Hippocampal Cornu Ammonis Pyramidal Neuron Excitability by Inhibition of Both Transient and Persistent Sodium Currents in Mice. Anesthesiology. 131:94-104.

Supplemental Figure 1

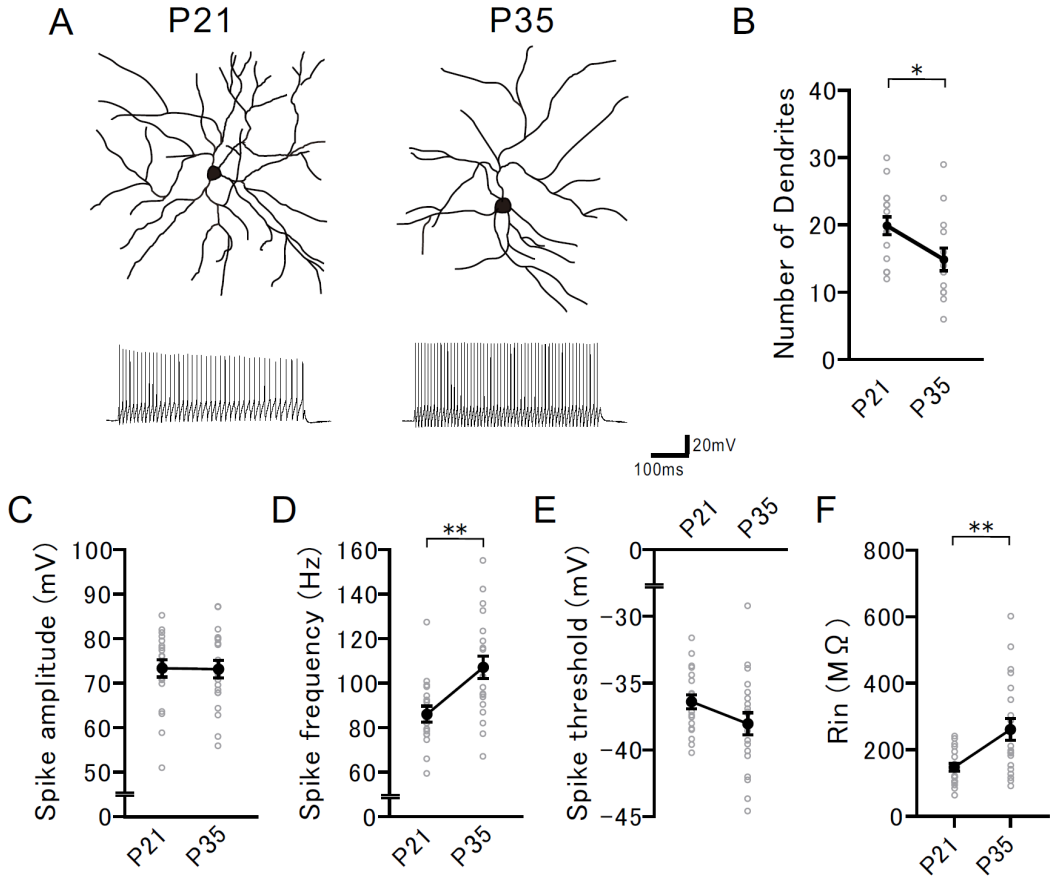

(A) Top: Reconstruction of PV cells recorded at P21 (left) and P35 (right). Bottom: representative spikes elicited by a current injection 100-pA lager than the rheobase recorded from PV cells at P21 (left) and P35 (right).

(B) The number of dendrites decreased with development (two-tailed *t*-test, t_{29} = 2.389, **P* = 0.0236, *n* = 17 (P21), 14 (P35)).

(C) Spike amplitude did not change with development (two-tailed *t*-test, t_{38} = 0.06366, *P* = 0.9496, *n* = 20 (P21), 20 (P35)).

(D) Spike frequency increased with development (two-tailed *t*-test, t_{36} = 3.286, ** *p* = 0.0023, *n* = 18 (P21), 20 (P35)).

(E) Spike threshold did not change with development (two-tailed *t*-test, t_{38} = 1.674, *P* = 0.1023, *n* = 20 (P21), 20 (P35)).

(F) Input resistance increased with development (Mann-Whitney *U* test, *U* = 103, ***P* = 0.0080, *n* = 20 (P21), 20 (P35)).

**P* < 0.05, ***P* < 0.01. Data are represented as means and error bars indicate SEM.

Supplemental Figure 2

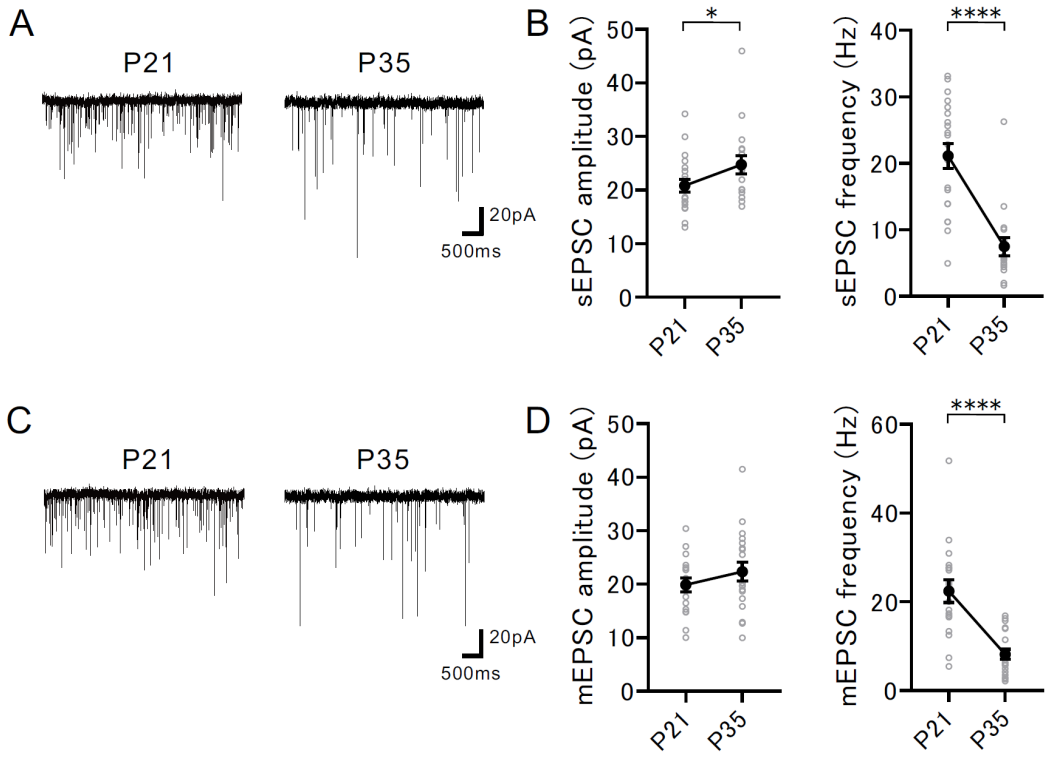

(A) Representative traces showing sEPSCs recorded from the PV cells at P21 (left) and P35 (right).

(B) Left: sEPSC amplitude significantly increased with development (Mann-Whitney *U* test, $U = 103$, $^{*}P = 0.0417$, $n = 20$ (P21), 17 (P35)). Right: sEPSC frequency significantly decreased with development (Mann-Whitney *U* test, $U = 30$, $^{****}P < 0.0001$, $n = 20$ (P21), 17 (P35)).

(C) Representative traces showing mEPSCs recorded from the PV cells at P21 (left) and P35 (right).

(D) Left: mEPSC amplitude did not change with development (two-tailed *t*-test, t_{35} = 1.119, p = 0.2708, n = 18 (P21), 19 (P35)). Right: mEPSC frequency significantly decreased with development (Mann-Whitney *U* test, U = 31, ****P < 0.0001, n = 18 (P21), 19 (P35)).

*P < 0.05, ****P < 0.0001. Data are represented as means and error bars indicate SEM.

Supplemental Figure 3

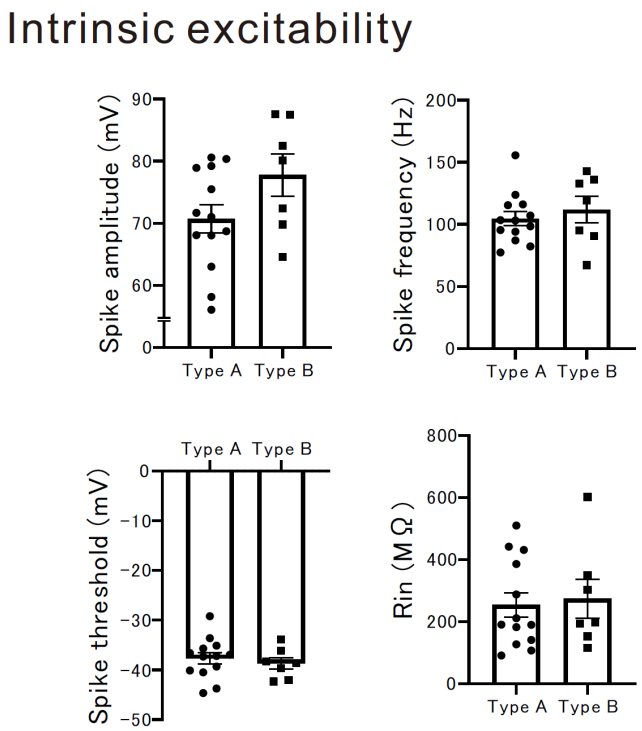

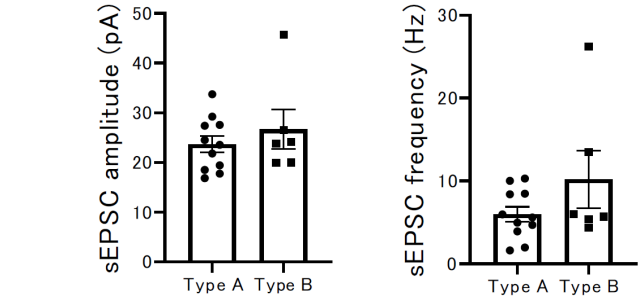

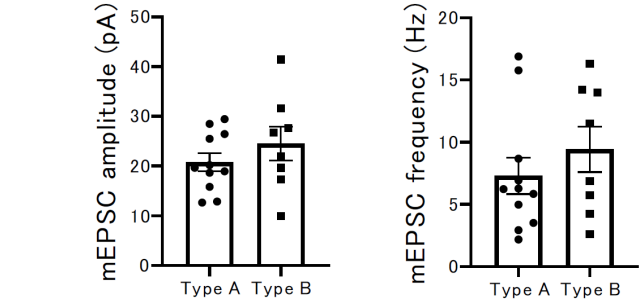

There were no differences in firing properties and EPSCs between type A and type B cells at P35. Spike amplitude (two-tailed *t*-test, t_{18} = 1.780, p = 0.0919, n = 13 (type A), 7 (type B)). Spike frequency (two-tailed *t*-test, t_{18} = 0.6812, p = 0.5044, n = 13 (type A), 7 (type B)). Spike threshold (two-tailed *t*-test, t_{18} = 0.5760, P = 0.5717, n = 13 (Type A), 7 (Type B)). Input resistance (two-tailed *t*-test, t_{18} = 0.2834, P = 0.7801, n = 13 (Type A), 7 (Type B)). sEPSC amplitudes (two-tailed *t*-test, t_{15} = 0.8398, P = 0.4142, n = 11 (type A), 6 (type B)). sEPSC frequency (two-tailed *t*-test, t_{15} = 1.510, p = 0.1519, n = 11 (type A), 6 (type B)). mEPSC amplitudes (two-tailed *t*-test, t_{17} = 1.054, P = 0.3067, n = 11 (type A), 8 (type B)). mEPSC frequency (two-tailed *t*-test, t_{17} = 0.9209, P = 0.3700, n = 11 (type A) and 8 (type B)).

Data are represented as means and error bars indicate SEM.